DEPARTMENT OF PHYSICS, UNIVERSITY OF JYVÄSKYLÄ
RESEARCH REPORT No. 1/1993

ELECTRONIC SHELL STRUCTURE IN LARGE METAL CLUSTERS

BY
JUHA MANSIKKA-AHO

Academic Dissertation
for the Degree of
Doctor of Philosophy

Jyväskylä, Finland
June 1993

URN:ISBN:978-951-39-9806-6
ISBN 978-951-39-9806-6 (PDF)
ISSN 0075-465X

Jyväskylän yliopisto, 2023

ISBN 951-34-0000-X
ISSN 0075-465X

DEPARTMENT OF PHYSICS, UNIVERSITY OF JYVÄSKYLÄ
RESEARCH REPORT No. 1/1993

ELECTRONIC SHELL STRUCTURE IN LARGE METAL CLUSTERS

BY
JUHA MANSIKKA-AHO

Academic Dissertation
for the Degree of
Doctor of Philosophy

To be presented, by permission of the
Faculty of Mathematics and Natural Sciences
of the University of Jyväskylä,
for public examination in Auditorium S-212 of the
University of Jyväskylä on June 4, 1993,
at 12 o'clock noon

Jyväskylä, Finland
June 1993

Preface

This thesis is based on studies carried out during years 1990-1993 at the Department of Physics of the University of Jyväskylä. I have been supervised by Prof. Matti Manninen and Dr. Esko Hammarén, to whom I wish to express my gratitude for numerous inspiring and encouraging discussions concerning my work. I would also like thank Prof. Hide Nishioka, Prof. Puru Jena and Prof. Shiv Khanna for a pleasant collaboration. I have benefited from a collaboration and discussion with Dr. Hannu Häkkinen, Dr. Seppo Valkealahti, Mr. Juha Merikoski, Dr. Jouni Suhonen and Prof. Pertti Lipas, as well as from the excellent working atmosphere created by the Solid State Group and the whole personnel of the Department. The financial support from the Academy of Finland is greatly acknowledged.

Jyväskylä, May 1993

Juha Mansikka-aho

Abstract

This thesis reviews six publications which investigate the effect of the surface on the electronic shell structure in large metal clusters. The Hückel model is used to study the shell structure and cluster geometry of fcc clusters. A tight binding model and the Monte Carlo technique is used to simulate metallic fcc clusters at finite temperatures for determining the level spacing distribution at the Fermi energy. A potential-well approximation is used to study the shell structure in cuboctahedral and icosahedral clusters and also to calculate the band structure in cluster-assembled materials. The Woods-Saxon potential has been used to study the effect of the softness of the surface potential on the shell structure. The main results are as follows: (i) The surface faceting destroys the shell structure in fcc clusters already when the cluster has of the order of 100 atoms. (ii) The icosahedral clusters have the same shell structure as the sphere up to about 1000 atoms. (iii) The surface roughness causes the level distribution to be a Wigner distribution. (iv) Using the Woods-Saxon potential a softness can be found where the shell structure is governed by the classical star orbit. However, real metal clusters are not soft enough to exhibit the signature of the star orbit. (v) If crystalline materials can be formed from magic metal clusters, they are expected to be semiconductors.

List of publications

This thesis is a review of the following publications:

I M. Manninen, J. Mansikka-aho and E. Hammarén, *Equivalence of the Shell Structure in Tight-Binding and Free-Electron Clusters*, Europhys. Lett. **15**, 423 (1991)
https://doi.org/10.1209/0295-5075/15/4/010

II J. Mansikka-aho, M. Manninen and E. Hammarén, *On the Shell Structure and Geometry of Monovalent Metal Clusters*, Z. Phys D - Atoms, Molecules and Clusters **21**, 271 (1991)
https://doi.org/10.1007/BF01426385

III J. Mansikka-aho, E. Hammarén and M. Manninen, *Shell Structure in large nonspherical Metal Clusters*, Phys. Rev. B. **46**, 12649 (1992)
https://doi.org/10.1103/PhysRevB.46.12649

IV J. Mansikka-aho, M. Manninen and E. Hammarén, *Level Spacing Distribution in the Tight Binding Model of Fcc Clusters*, JYFL Preprint 11/92, Phys. Rev. B., in press
https://doi.org/10.1103/PhysRevB.47.10675

V M. Manninen, J. Mansikka-aho, S. N. Khanna and P. Jena, *Band Structures of Solids Composed of Metal Clusters*, Solid State Comm. **85**, 11 (1993)
https://doi.org/10.1016/0038-1098(93)90908-6

VI J. Mansikka-aho, M. Manninen and H. Nishioka, *Star Orbits in Metal Clusters*, JYFL Preprint 1/93, submitted to Phys. Rev. B.
https://doi.org/10.1103/PhysRevB.48.1837

The author has written the first manuscript of all the papers, except **I** and **V**. All the computations have been done by the author, except the self-consistent jellium model calculations in **VI**.

Table of contents

1. Introduction

Atomic clusters are a new class of many-body systems. The atoms are held together by the cohesive forces, and usually, the atoms are of the same element. As a consequence of the weak cohesive force, the cluster can easily lose a single atom or break up to a few small clusters. Generally, the clusters do not have the same structure as the bulk solid and the electronic properties of the clusters can differ remarkably from those of the bulk solid. One aim of the investigation of the atomic clusters is to follow the change of the different properties as a function of the cluster size from a single atom to the bulk solid. Many properties then depend on the ratio of the number of surface atoms to the total number of atoms.

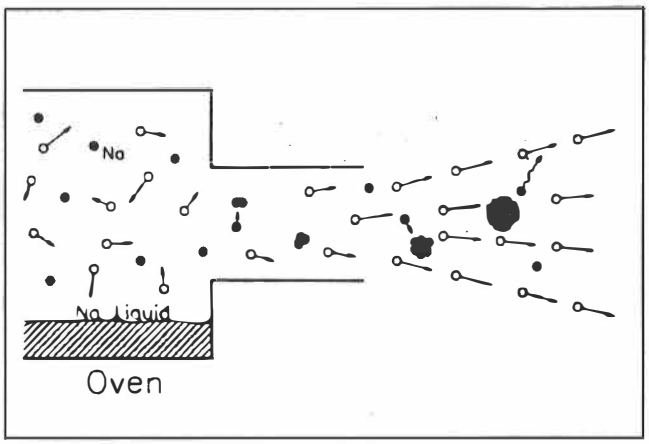

Fig. 1. Production of sodium clusters [from Ref. 1].

A typical experiment is shown in Fig. 1. The cluster source consist of a hot oven from which sodium liquid will escape by simple evaporation. Sodium vapour is held at 700 – 800 °C. The vapour is allowed to mix with a cold, inert noble gas. The mixture is expanded into a vacuum and the vapour particles will condense into clusters, resulting a narrow beam. The resulting internal temperature in the freshly formed clusters is supposed to be just some 100 – 200 °C below the oven

temperature. In the ensuing free flight the droplets will therefore loose sodium atoms by stepwise evaporation, cooling to about 100 – 200 °C. This evaporation process is sensitive to shell-like variations in the atomic separation energies. These variations are thought to be responsible for the step-like modifications of the experimentally observed size distributions. The size distribution of the clusters can be controlled by varying the oven-to-nozzle distance, the gas pressure and the oven temperature. The size distribution can be sampled by time-of-flight mass spectrometry[2].

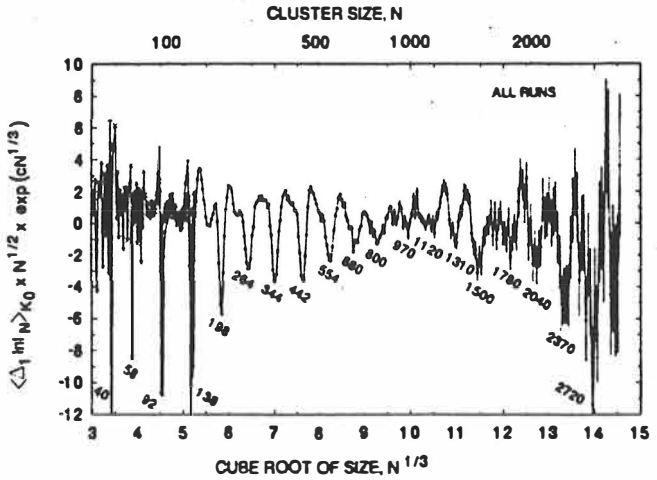

Fig. 2. The experimental shell structure for sodium [from Ref. 1].

Fig. 2 shows an experimental cluster abundance I_N obtained in this way[1]. In order to compensate for the effect of temperature and size, a weighted logarithmic derivatives, $<\Delta_1 \ln I_N>_{K_0}$ [1], have been scaled with the factor $N^{\frac{1}{2}}\exp(cN^{\frac{1}{3}})$, setting $c = 0.65$. The results have been plotted as a function of linear dimensions of the clusters, $\sim N^{\frac{1}{3}}$. The shell dips are equidistantly spaced. The numbers below the minimums are the experimental magic numbers for sodium. Recently, the experimental research has been done abundantly[1,3 – 12].

The conduction electrons in a simple metal form almost a free electron gas. Many properties of metals can be explained by examining the homogeneous electron gas. The simplest model for the electronic structure of the alkali metal clusters is the jellium model[13 – 16]. In that model the metal ions are replaced by

a fixed homogeneous positive background distribution, which has the same density as the conduction electrons. In the spherical jellium model the background density is a homogeneous sphere. This model explains qualitatively the magic numbers observed in the experimental abundance spectrum[17,18]. They represent the filling of electron shells in the spherical potential well.

The shell structure is defined as large energy gaps between the energy levels. In 1949 Goeppert-Mayer [19] and Haxel, Jensen and Suess [20] observed the shell structure to explain the stability of the magic numbers in the atomic nuclei. The electrons in the metal clusters have been described with the same kind of model since the first experiments. The magic numbers of the atomic nuclei differ from the atomic clusters. In 1984 Knight et al. [21] did the first experimental research for the shell structure and found the magic numbers for the sodium clusters. Later the shell structure was investigated also for K-[17,22], Cu-, Ag- and Au-clusters[23]. Shell structures were observed for the small metal clusters with less than 100 atoms. Recently, the electronic shell structure has been investigated experimentally up to 3000 atoms[4] and the mass spectrum for sodium have been observed up to 22000 atoms[3].

Both experimental and theoretical shell closings and gaps show oscillations according to scale $N^{\frac{1}{3}}$ in the shell structure, where N is the number of electrons. The bunches of the electron shells form long-range oscillations called supershells. This was first predicted by Balian and Bloch[24] using a spherical cavity as a potential well. The supershell structures can be seen only in clusters with more than 1000 atoms. The intensity variation and phase shift of the supershell structure, was predicted by Nishioka et. al.[25]. In 1991 the existence of the supershells in sodium clusters was experimentally observed[4] (see Fig. 2). The effect of temperature on the supershell structure in large sodium clusters has also been investigated[26] and it was observed that the amplitude of the shell structure decreases with increasing temperature.

The self-consistent jellium model explains well the experimentally observed supershell structure[27]. Genzken et. al.[28] have done the self-consistent calculations of the supershell structure and observed the agreement with the experimental

results to be very good for the alkali metal clusters but poor in the case of aluminium. However, it is often more illustrative to use the semiclassical interpretation where the supershell structure is a result from the interference of classical orbits. The effect of the interference arises from the difference of the lengths of the orbits. Recently, the simplified semiclassical theory for the electronic shell structure have been presented[29] by extending the semiclassical analysis by Balian and Bloch. The detailed shell structure is sensitive to the shape of the potential. Lerme et. al.[5,6] have suggested that the mass spectrum they have measured for Al could be explained by an electronic shell structure in a soft potential well. The aluminium requires an electron orbit twice as long as that needed to explain the electronic shells in a sodium. This can be explained with a classical star orbit. However, Genzken et. al.[28] indicate that in Al the electronic shell structure does not have a signature of the classical star orbit. The experimental evidence of the star orbit is still in doubt, since Martin et. al.[7] has shown that the observed shell structure can be explained with a geometrical packing of Al atoms in octahedral clusters. The relation of the classical star-orbit to the quantum mechanical level structure is studied in Section 5. We have shown that for a soft potential the star orbit indeed dominates the shell structure, but this is not the explanation to the experimental results for Al clusters.

The spherically symmetric potential of the jellium model leads to a large degeneracy of the electron states corresponding to high angular momentum eigenvalues. In real clusters the effective potential is not strictly spherical while it is affected by the ionic structure. In 1991 the icosahedral symmetry was observed in the large magnesium clusters[8]. Group theory dictates that the maximum degeneracy is five for the icosahedron structure[30]. In sodium clusters magic numbers corresponding to the icosahedral packing have been observed in addition to the electronic magic numbers. In this thesis we have studied the possibility of the existence of the electronic shell structure in icosahedral and other faceted clusters. It is shown that the electronic shell structure is totally destroyed by the icosahedral symmetry only when the cluster has more than 1000 atoms.

At finite temperatures many properties of metals depend on the density of states at the Fermi level. In clusters we have discrete energy levels and then

the important quantity will be the average level spacing at the Fermi level. The statistical distribution of level spacings determines the physical properties like the electronic specific heat[31]. We have developed a tight binding model for studying the level spacing statistics. The results show that the distribution is always a Wigner distribution, and the width of the distribution depends on the cluster size and temperature.

Atomic clusters can serve as a source of new materials with unusual properties[32]. Recently, it was suggested[33] that a crystalline structure could be assemled from the magic metal clusters. The clusters would be weakly bound to each other and form a close packed structure like fcc. A nonmetallic example of this kind material is the solid fullerene[34,35] where the fullerene molecules are bound together with van der Waals interactions. Jena and Khanna[33] suggested $Al_{12}Si$ as a candidate of clusters which could be used in assembling new materials. It has a compact icosahedron geometry and closed electronic shell due to its 40 valence electrons. The key question for the possibility of weakly bonded cluster material is the existence of narrow energy bands. To this end we have made model calculations for the band structures of materials assembled of metal clusters.

2. Hückel clusters and the shell structure

2.1. Formalism of the Hückel model

For calculating the electronic structure we need in many cases a model which takes into account the actual atomic positions. The tight binding model is perhaps the simplest such model. In the Hückel model[36] the overlap of orbitals from neighbouring atoms is neglected. The resonance integrals are nonzero only for nearest neighbours. The electron energy levels are eigenvalues of the matrix

$$H_{ii} = \alpha$$
$$H_{ij} = \begin{cases} -\beta & \text{if i and j are nearest neighbours} \\ 0 & \text{otherwise} \end{cases} \qquad (1)$$

where α and β are the Hückel Coulomb and resonance integrals, respectively. In practise, the parameter α gives a constant shift in the energy spectrum and β its scale. At an infinite crystal the energy eigenvalue $\epsilon(\mathbf{k})$ is

$$\epsilon(\mathbf{k}) = \alpha - \beta \sum_{\text{n.n.}} \exp(i\mathbf{k} \cdot \mathbf{r}), \tag{2}$$

where $\mathbf{k}$ is the wave vector and the sum runs over all nearest neighbour sites $\mathbf{r}$. For example, in fcc lattice $\mathbf{k} \cdot \mathbf{r} = \frac{1}{2}a(\pm k_i, \pm k_j)$ and i,j = x,y; y,z; z,x. The parameter a is the lattice constant.

For a cluster the one-electron energy eigenvalues are determined numerically by diagonalising the Hückel matrix. The energy units are chosen to be the Hückel units (hu), where $\alpha = 0$ and $\beta = 1$. The total energy is the sum of the energies of the occupied one electron energy levels. Each energy level can occupy two electrons so that in the neutral clusters half of the energy levels are filled. The energy eigenvalues for the bulk (Eq. (2)) are between -12β and 4β in the fcc lattice. Lindsay et. al.[37 – 40] have investigated the application of the Hückel model for small clusters. We have studied the shell structure in the large clusters with different geometries[41].

2.2. Relation of the Hückel model to the free electron model

The simplest free electron model for the metal clusters is the spherical potential box with hard walls. The radial electron wavefunctions are the spherical Bessel functions. We can easily solve the level structure from the zeroes of these functions. For small clusters this model gives the same kind of shell structure as observed experimentally for all monovalent metals. We will now show that the Hückel model gives the same shell structure as the free electron model.

The Schrödinger equation of the free electron model is

$$-\frac{\hbar^2}{2m}\nabla^2\psi(\mathbf{r}) = \epsilon\psi(\mathbf{r}). \tag{3}$$

By discretizing the wave function in a cubic grid (for numerical solution) we write $\nabla^2\psi$ as

$$\nabla^2\psi(\mathbf{r}_i) \rightarrow \frac{1}{a^2}\left(\sum_j^{n.n.}\psi_j - c\psi_i\right), \tag{4}$$

where $\mathbf{r}_i$ is a grid point, $\psi_i = \psi(\mathbf{r}_i)$, a the lattice constant, and c the coordination number (12 for fcc). The Schrödinger equation can now be written as a set of linear homogeneous equations:

$$\frac{\hbar^2 c}{2ma^2}\psi_i - \frac{\hbar^2}{2ma^2}\sum_j^{n.n.}\psi_j = \epsilon\psi_i. \tag{5}$$

When these equations are written in the matrix form the Hamiltonian matrix is equal to the Hückel matrix of eq. (1), with

$$\alpha = \frac{\hbar^2 c}{2ma^2}, \qquad \beta = \frac{\hbar^2}{2ma^2}. \tag{6}$$

This shows that in the cubic mesh the discretized free electron model is the same as the Hückel model.

The Hückel model takes a to be the actual lattice constant in the solid. This means that the corresponding free electron model is accurate only for states with wavelength long compared to the nearest neighbour distance (for the lowest energy states). For a bulk lattice this means that $\epsilon(\mathbf{k})$ is isotropic at small $\mathbf{k}$ [42]. In the tight binding model the electron wave function is zero outside the cluster where there are no atoms. This corresponds to a hard wall potential at the surface of the free electron clusters. For spherical clusters the lowest energy levels of the Hückel model are equivalent to the energy levels in a spherical potential box with hard walls.

2.3. Shell structure of spherical Hückel clusters

The discrete energy levels of the cluster move slowly and continuously towards the bottom of the band when the cluster size increases. At the same time the mutual distance between the energy levels decreases and the subshell structure will cause the mixing of the energy levels. The shell structure is determined to large energy gaps between the energy levels. Generally, the shell structure for metal clusters is based on the assumption that the valence electrons are almost free and they move in the nearly constant potential caused by positive ions. The number of the electrons occupying the states below the large energy gap in the shell structure is called a magic number. The magic numbers for the clusters are analogous with nuclear magic numbers. For the nuclei these numbers correspond to the numbers of neutrons and protons for which the nuclei are particularly stable. In the clusters the magic numbers reflect shell closings arising from the quantisation of the motion of delocalized electrons in a mean-field potential of high symmetry.

The spherical clusters are cut off from the fcc lattice so that one atom is in the center of the cluster. The density of states ρ can be used to study the shell structure. In order to better visualise the shell structure the discrete levels have been convoluted with a Lorenzian

$$\rho(\epsilon) = \sum_{\nu} \frac{\Gamma}{(\epsilon - \epsilon_\nu)^2 + \Gamma^2} \tag{7}$$

where ϵ_ν are the energy eigenvalues. A suitable width is $\Gamma = 0.1\beta$, which is about $\frac{1}{10}$ of the energy gap between the energy shells. This width does not have any physical meaning. Figure 3a shows the density of states for free electrons in a spherical potential box. This is compared to the density of states for a Hückel cluster containing 959 atoms in Fig. 3b. Well below the Fermi energy the overall structure of the Hückel density of states is similar to the electronic shell structure of free electrons in a spherical box. This is a consequence of the same Hamiltonian.

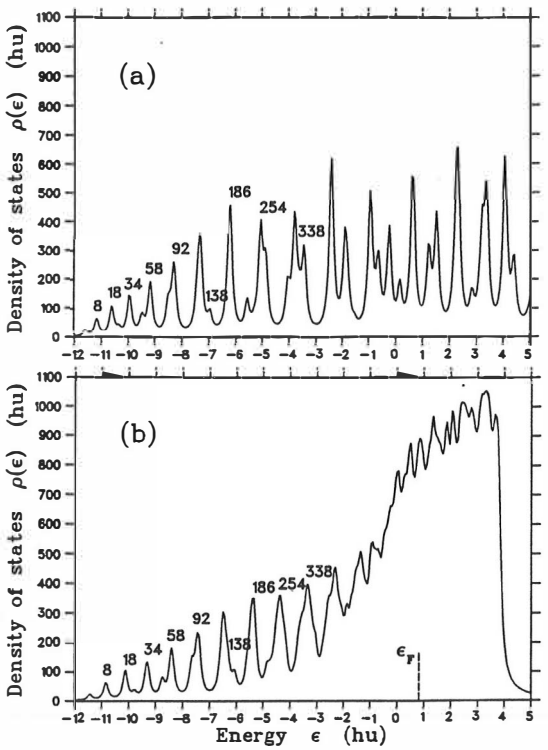

Fig. 3. **a)** Density of states for free electrons in a spherical potential box and **b)** for a spherical Hückel cluster of 959 atoms. The numbers above the peaks indicate the total number of electrons at various shell closings. The Fermi energy of the Hückel cluster is denoted by ϵ_F.

When the cluster size increases more and more discrete energy shells are visible in the Hückel model. This is also clearly seen in the results of Lindsay et. al.[40].

The highest energy levels of the Hückel model are very different from those of the free-electron model. They have condensed to one bunch in the Hückel model whereas in the free electron model they are clearly separate electron energy shells. Already near the Fermi energy there is a large difference between the two models. We can see from Fig. 3 that the fcc Hückel model gives the correct free electron shell structure at least up to the shell filling 338 which covers about one third of the states below the Fermi level. A similar result has been obtained for cube-shaped clusters[43]. The shell structure for cube-shaped clusters does not remind the shell structure in the spherical case, but low energy levels are the same for both models.

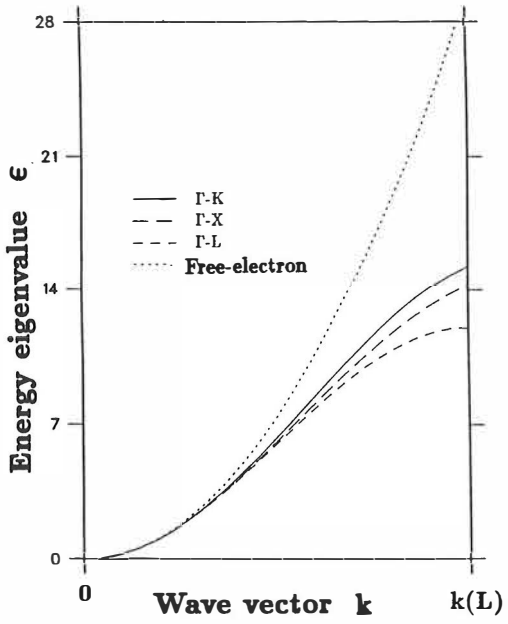

Fig. 4. Band structure for the fcc lattice. The simple Hückel model for three main crystal directions and the free electron parabola.

Messmer[44] has utilized that by studying the electron structure as a function of the cluster size and of the width of the band in the Hückel model.

Figure 4 shows the tight binding energy bands in the (100), (110) and (111) directions in the standard Hückel model and the free electron energy eigenvalue as a function of the wave vector **k**. The free electron energy eigenvalue and the Hückel energy band coincide for small **k**-values. The energies depart from each other slowly with increasing **k** and for the high energies the models are entirely different. The simple Hückel model is an approximation for the free electron model only at small **k**-values.

2.4. Effects of the geometry on the shell structure

Polyhedral clusters with an fcc lattice structure can be easily studied with the Hückel model. Examples of different geometries are shown in Fig. 5. The

cubo-octahedron consists of 8 triangular (111) faces and 6 square (100) faces. The octahedron consists of 8 triangular (111) faces. The Wulff polyhedron has been formed from an octahedron with 1156 atoms by removing three layers of atoms from each corner. The Wulff polyhedron minimizes the total energy of an asymptotically large cluster.

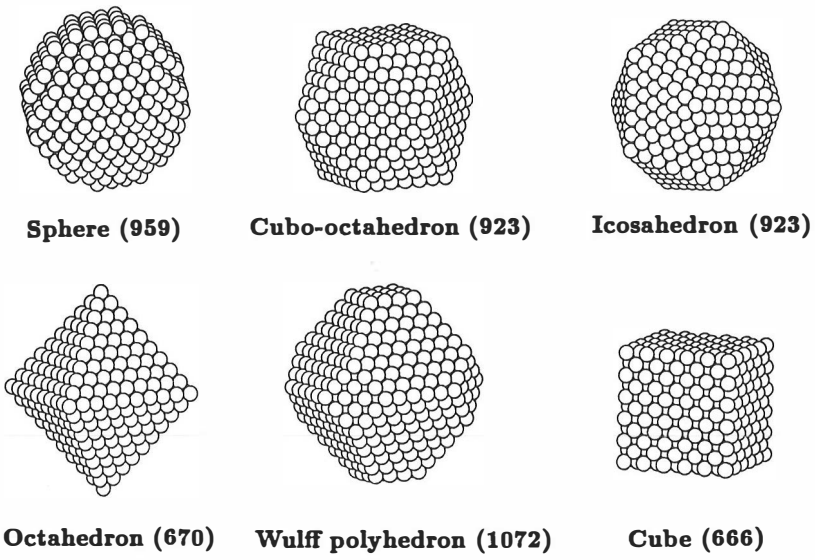

Fig. 5. Examples of cluster geometries studied. The number inside of brackets indicates the number of atoms in cluster.

An icosahedron cannot be formed from the fcc lattice; there are two different distances between neighbouring atoms in the icosahedral structure. However, we assume that the resonance integral β has the same value for both of these distances. Icosahedron consists of twenty triangular (111) faces. The density of atoms and the number of nearest neighbours are largest on (111) face in fcc lattice. The total energy for the structure which consists of these faces is generally smaller than that for the geometries formed from the other faces. The icosahedral cluster is the most spherical of all the faceted clusters considered.

Figure 6 shows densities of states for different cluster geometries calculated with Hückel model. The shell structure for a sphere is seen in Fig. 3b. The shell structure clearly visible in the spherical cluster is almost completely missing in

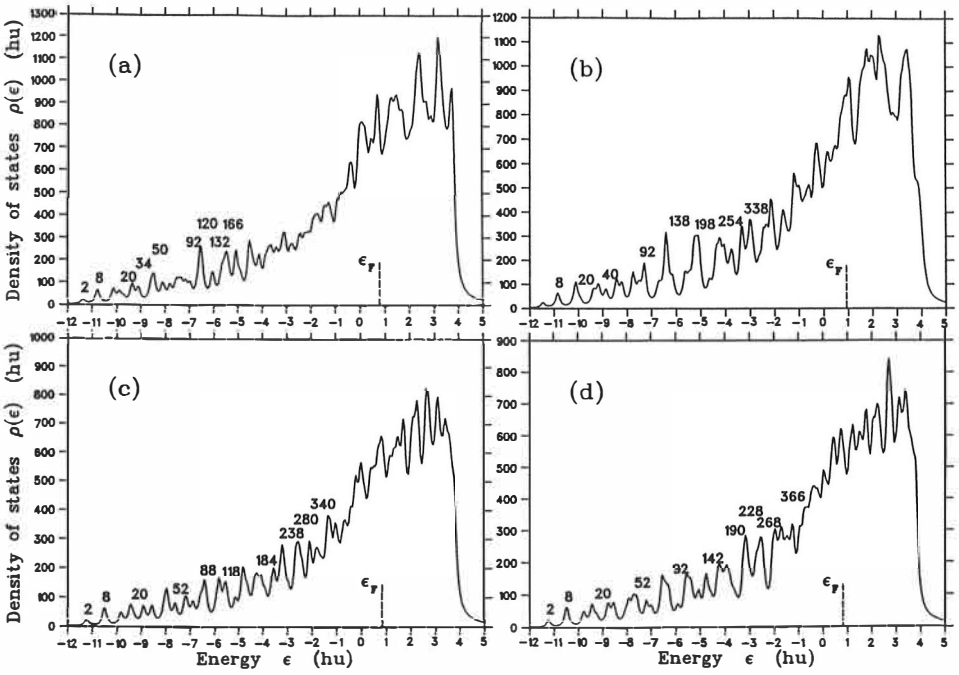

Fig. 6. Density of states of Hückel clusters with different geometries. **a)** Cubo-octahedron (923). **b)** Icosahedron (923). **c)** Octahedron (670). **d)** Wulff polyhedron (640).

the cubo-octahedral cluster. On the contrary the icosahedral cluster of about one thousand atoms shows a free electron shell structure similar to that of the spherical cluster at least up to a few hundreds of electrons. When the cluster size increases the number of the shells having free electron character increases. However, the increase of the visible electron shells is slower than the increase of the cluster size.

The icosahedral cluster has not an fcc packing of atoms. Consequently, the Hückel model is not exactly the same as the free electron model even for the lowest electron states. This is due to the slightly different distances between the different nearest neighbours. However, the results suggest that the approximation is still valid and that the icosahedral cluster will have the free electron shell structure. There is experimental evidence[3] about icosahedral structure for larger clusters, but the shell structure have not been observed simultaneously, yet.

The shell structure for the octahedron and for the cube is very different from that of a sphere. The Wulff construction shows more features of the shell structure

of the free electron sphere but even there the shell structure is different already at very low energies. In conclusion, the faceting of the surface of the fcc clusters destroys the shell structure of nearly free electron metal clusters already when the cluster size is about 100 electrons or less. The result seems to indicate that large alkali metal clusters with observed magic numbers do not have crystalline packing with a polyhedron shape. The only possible exception is the icosahedral structure, where according to these results the shell structure should persist up to cluster sizes of at least hundreds of atoms.

2.5. Beyond the nearest neighbour interaction in the Hückel model

In the simple Hückel model only the nearest neighbour resonance integrals are nonzero. The model can be extended by allowing the parameter β to be distance dependent. First we will demonstrate that the relation between the Hückel model and the free electron model can be made more accurate by a proper choice of the distance dependence of β. Secondly, we will study an exponential distance dependence of β.

Better approximation for $\nabla^2\psi$ than that in Sect. 2.2 can be obtained if more lattice points are used. Including the second and the third neighbours the wave vector ψ_j can be developed as a series, which consist of partial derivatives of ψ_i with respect to x-, y- and z-axes in the fcc lattice. By including the terms up to the 4th power we can derive an estimate

$$\nabla^2\psi_i = \frac{1}{24a^2}\left(18\sum_j^{1n.n.}\psi_j - \sum_j^{3n.n.}\psi_j - 192\psi_i\right), \tag{8}$$

where the first sum goes over the first nearest neighbours and the second one over the third nearest neighbours. The sum over the second nearest neighbours is zero.

This discretization is equal to the Hückel model where

$$H_{ij} = \begin{cases} \frac{192}{24}\frac{\hbar^2}{2ma^2}, & \text{if } i = j, \\ -\frac{18}{24}\frac{\hbar^2}{2ma^2}, & \text{if } i \text{ and } j \text{ nearest neighbours,} \\ \frac{1}{24}\frac{\hbar^2}{2ma^2}, & \text{if } i \text{ and } j \text{ third neighbours,} \\ 0 & \text{otherwise.} \end{cases} \tag{9}$$

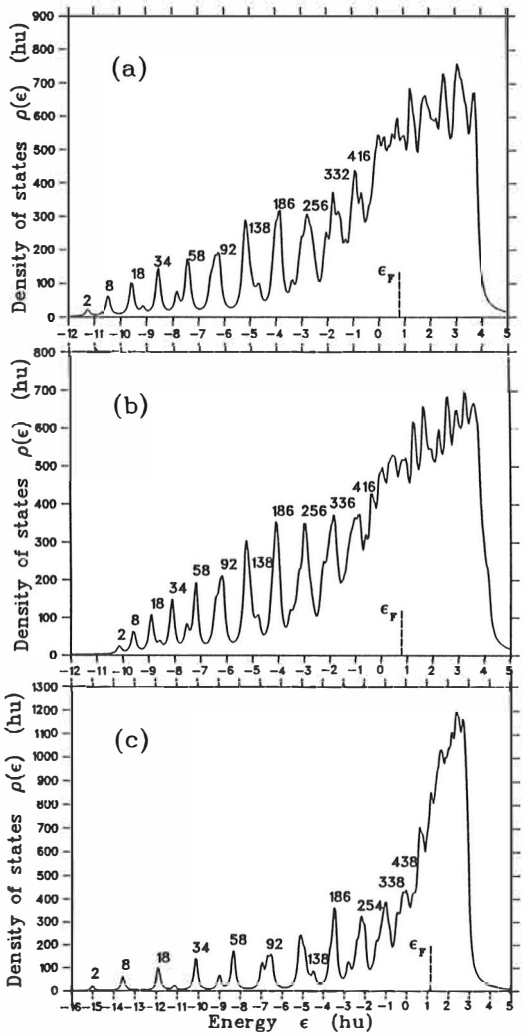

Fig. 7. Density of states for a sphere with 627 atoms. **a)** Hückel model with nearest neighbour interactions, **b)** third nearest neighbour interactions included and **c)** Hückel model with exponential distance dependence with $\eta = 0.5$.

Figure 7 demonstrates the effect of this correction to the Hückel shell structure. The correction sharpens the peaks of the shell structure at small energies, but that effect does not extend the appearance of discrete shells closer to the Fermi surface. The third neighbour approximation does improve the estimate of the Laplace operator $\nabla^2\psi$ at long wavelengths, but it is not adequate when the wavelength becomes comparable to the lattice constant. The tight binding method (Hückel) with the overlap of orbitals considered up to third nearest neighbours have been used to describe the surface roughness of a cluster[45].

We have also tried an exponential distance dependence for the atom-atom interaction. The Hückel matrix elements are

$$H_{ij} = -\beta \exp[-\eta(d - d_{nn})] \tag{10}$$

where η is a coefficient for the distance dependence, d is the distance between the atoms and d_{nn} is the nearest neighbour distance. In the case of an fcc lattice the $\eta \rightarrow \infty$ limit recovers the original Hückel model.

Figure 7c shows the effects of the exponential distance dependence with η = 0.5 on the electronic structure of sphere (627). The energies of the low lying states fall below -12β, which is the lowest energy in original Hückel model. The separation between low energy levels increases but the high lying levels stack more tightly together. The shell structure extends closer to the Fermi energy than in the simple Hückel model. This can be understood by comparing the free electron parabola to distance dependent Hückel band structure (like in Fig. 4). The energies depart from each other slowly with increasing **k** and for the high energies the models are entirely different. The energy dispersion of the tight binding bands becomes smaller when η decreases. A smaller energy dispersion means a smaller crystal field splitting[46]. This explains why the shell structure is more clearly seen with smaller η.

2.6. Total energy of Hückel clusters

In the Hückel model the total energy is defined as a sum of the energy eigenvalues below the Fermi energy. The lower is the total energy the more stable is the structure. The total energy per atom as a function of the cluster size is shown in Fig. 8 for several geometries. The total energy of spherical clusters oscillates strongly due to the roughness of the surface. The lines in Fig. 8 approach the asymptotic limit as the size of cluster increases to infinity. The asymptotic limit is the cohesive energy of the fcc lattice, which in the Hückel model is $E_c = -2.62$ hu. The exception is the icosahedral structure for which asymptotic limit is different. In general, the large departure of total energy from the asymptotic value can be accounted for by the surface energy. When the size of cluster becomes larger the area of the surface increases, but the ratio of surface atoms to the bulk atoms decreases. That reduction of the ratio changes total energy toward the asymptotic limit. Including the surface energy the total energy per atom in large spherical clusters can be written as

$$\frac{E(N)}{N} = E_c + Ka^2\sigma N^{-\frac{1}{3}} \tag{11}$$

where K is a geometrical constant ($K = 1.9192$), a the lattice constant and σ the surface energy (in units of hu/a^2).

The surface energies in the Hückel model can be calculated using the moment method[47,48] to derive the local density of states. The projected density of states $g_i(\epsilon)$ which corresponds to local density of states can be calculated in tight binding model (Hückel model) without calculating the proper wave functions. The n^{th} moment of the density of states for an atom i can be defined as an integral

$$\mu_i^{(n)} = \int_{-\infty}^{\infty} d\epsilon\, \epsilon^n g_i(\epsilon). \tag{12}$$

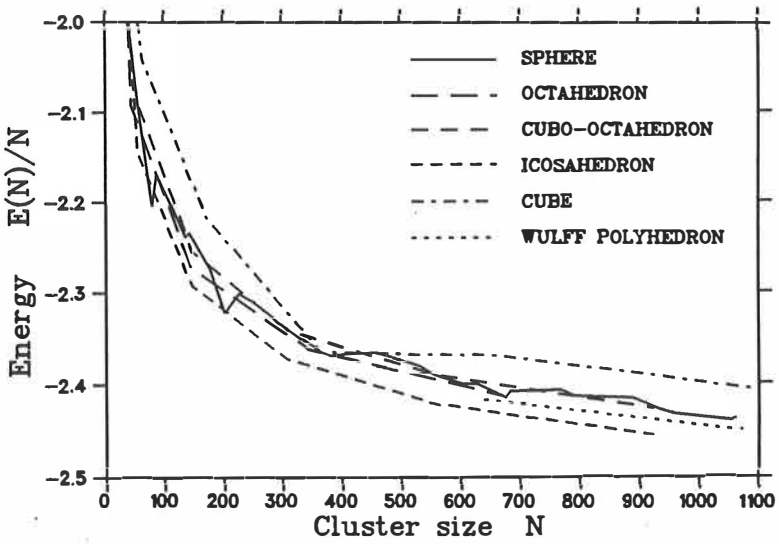

Fig. 8. Total energy per atom for different cluster geometries as a function of number of atoms N.

In practice the moment can be calculated from the Hamiltonian matrix:

$$\mu_i^{(n)} = \sum_{j_1} \sum_{j_2} \cdots \sum_{j_{n-1}} H_{ij_1} H_{j_1 j_2} \cdots H_{j_{n-1} i}. \tag{13}$$

The matrix elements of Hamiltonian are nonzero only for the orbitals between nearest neighbours. Graphically, the moments can be calculated by combining n nearest neighbours, starting from the lattice site i and finishing to the same place. It is sufficient to compute the moments up to $n = 8$[49]. The moments for a bulk atom are shown in Table I.

The density of states $g_i(\epsilon)$ can be estimated with the polynomial expansion

$$g_i(\epsilon) = \gamma_1(\epsilon - \epsilon_{\min})^{\frac{1}{2}} + \sum_{k=2}^{9} \gamma_k(\epsilon - \epsilon_{\min})^k, \tag{14}$$

where $\epsilon_{\min}$ is the bottom of the band (-12 hu). The coefficients γ can be calculated by combining Eq. (12) and (14) to nine different equations (one for each moment).

Table I. The moments up to $n = 8$.

Moment	
$\mu_i^{(0)}$	1
$\mu_i^{(1)}$	0
$\mu_i^{(2)}$	12
$\mu_i^{(3)}$	−48
$\mu_i^{(4)}$	540
$\mu_i^{(5)}$	−4320
$\mu_i^{(6)}$	42240
$\mu_i^{(7)}$	−403200
$\mu_i^{(8)}$	4038300

The surface energy per surface atom is

$$\sigma = \sum_m \int_0^{\epsilon_F} d\epsilon\, \epsilon[g_m(\epsilon) - g_b(\epsilon)], \tag{15}$$

where m denotes the atomic layer and g_b is the local density of states in the bulk.

The surface energies for the three most tightly packed fcc surfaces are given in Table II. The Wulff polyhedron (Fig. 5) is constructed by minimizing the surface energy of an infinitely large polyhedron. It consist of (111) and (100) surfaces, and can be obtained from the octahedron by cutting off the corners. Figure 8 shows that the total energy is smaller in that structure than in any other fcc cluster with the same size. This indicates that if the lattice structure is restricted to be an fcc, Hückel clusters will have their asymptotic geometry already when the cluster has about 600 atoms. Total energies of large icosahedral clusters are lower than those having an fcc packing. However, there is no quarantee that the icosahedral geometries are the

Table II. Surface energies in the Hückel model for the fcc structure.

Surface	Surface energy (hu/a^2)
111	0.76
100	1.00
110	1.01

actual ground states of the mathematical Hückel model. It is interesting to note that also in the Lennard-Jones clusters the icosahedral geometries are more stable than the spherical or cubo-octahedral clusters[50,51]. However, when a Lennard-Jones cluster has more than 1600 atoms a truncated decahedron seems to be the energetically favoured geometry[52].

3. Effect of surface roughness and the level spacing distribution in clusters

3.1. Energy levels and the surface roughness

The effect of the surface roughness is different for each individual cluster at a given time but the experiments measure only average properties over a large cluster ensemble. This leads to a statistical analysis of the level spectrum. The statistics of the level structure may play an important role in experiments where the information is gathered from a large number of clusters[31,53]. In nuclear physics the level statistics is used also in analyzing complicated spectra[54]. Theoretical work has been mainly based on the random matrix theory[55,56], which e.g. has been used to determine the electronic contribution to the specific heat and the magnetic susceptibility[31]. It should be noted that in the nuclear physics the level spacing distributions are extracted from the excitation spectra corresponding to quantum mechanical many-particle states, whereas in the atomic clusters the distribution of

single particle levels in the immediate vicinity of the Fermi level is important in determining thermodynamic properties. In many experiments the size of the cluster is not exactly determined and the cluster ensemble contains a distribution of different sizes.

In order to be able to compute the level structure of a large number of clusters a simple model of lattice gas with a tight binding electronic structure is used. In the lattice gas model the sites of atoms form a uniform lattice but the occupation of lattice sites depends on the temperature. The lattice gas model has been extensively used to study plane surfaces of solids. A roughening transition will happen at the plane surface, when the free energy disappears. The free energy is connected to the formation of surface-steps and the surface becomes rough almost in a macroscopic scale. In the clusters we are interested in the small scale roughness and do not study the rougening transition. At a finite temperature the surface shape can vary from cluster to cluster. The change of the surface structure changes the energy levels.

3.2. sp-Hückel model

A Hückel band structure for s-electrons does not correspond well to a free electron band structure. The simple Hückel model has anisotropic energy bands which destroy the shell structure[43]. The inclusion of long-range interactions and overlap-integrals can reduce the anisotropy but they do not reduce the density of states at the Fermi level[41,45]. Thus, the simple Hückel model is not a good approximation for the free electron model at the Fermi surface. However, the simple Hückel model can be improved by including more than one energy level for each atom. This can be done by taking linear combinations of s- and p-orbitals for each atom. This gives more freedom for the band structure and the parameters can be fitted to give a s-electron band which corresponds to the free electron parabola below the Fermi energy. We have done this for the fcc structure, and used the obtained parameters to compute level structures of clusters. The calculated magic numbers

correspond well to the free electron magic numbers below the Fermi energy. We will call this model the sp-model.

In the sp-model the overlap integrals are neglected and only nearest neighbour resonance integrals are assumed to be nonzero. For the bulk metal each element in the simple Hückel Hamiltonian matrix is replaced by the following 4 × 4 Hermitian matrix[42]:

$$
\begin{aligned}
H_{11} &= \gamma_0 \cos(\tfrac{1}{2}k_x a)\cos(\tfrac{1}{2}k_y a) + \gamma_0 \cos(\tfrac{1}{2}k_y a)\cos(\tfrac{1}{2}k_z a) + \gamma_0 \cos(\tfrac{1}{2}k_z a)\cos(\tfrac{1}{2}k_x a),\\
H_{22} &= E_p + \gamma_1 \cos(\tfrac{1}{2}k_x a)\cos(\tfrac{1}{2}k_y a) + \gamma_1 \cos(\tfrac{1}{2}k_z a)\cos(\tfrac{1}{2}k_x a) + \gamma_2 \cos(\tfrac{1}{2}k_y a)\cos(\tfrac{1}{2}k_z a),\\
H_{33} &= E_p + \gamma_1 \cos(\tfrac{1}{2}k_y a)\cos(\tfrac{1}{2}k_z a) + \gamma_1 \cos(\tfrac{1}{2}k_z a)\cos(\tfrac{1}{2}k_y a) + \gamma_2 \cos(\tfrac{1}{2}k_z a)\cos(\tfrac{1}{2}k_x a),\\
H_{44} &= E_p + \gamma_1 \cos(\tfrac{1}{2}k_z a)\cos(\tfrac{1}{2}k_x a) + \gamma_1 \cos(\tfrac{1}{2}k_y a)\cos(\tfrac{1}{2}k_z a) + \gamma_2 \cos(\tfrac{1}{2}k_x a)\cos(\tfrac{1}{2}k_y a),\\
H_{12} &= i\gamma_3 \sin(\tfrac{1}{2}k_x a)\cos(\tfrac{1}{2}k_y a) + i\gamma_3 \sin(\tfrac{1}{2}k_z a)\cos(\tfrac{1}{2}k_z a),\\
H_{13} &= i\gamma_3 \sin(\tfrac{1}{2}k_y a)\cos(\tfrac{1}{2}k_z a) + i\gamma_3 \sin(\tfrac{1}{2}k_y a)\cos(\tfrac{1}{2}k_x a),\\
H_{14} &= i\gamma_3 \sin(\tfrac{1}{2}k_z a)\cos(\tfrac{1}{2}k_x a) + i\gamma_3 \sin(\tfrac{1}{2}k_z a)\cos(\tfrac{1}{2}k_y a),\\
H_{23} &= -\gamma_4 \sin(\tfrac{1}{2}k_x a)\sin(\tfrac{1}{2}k_y a),\\
H_{24} &= -\gamma_4 \sin(\tfrac{1}{2}k_x a)\sin(\tfrac{1}{2}k_z a),\\
H_{34} &= -\gamma_4 \sin(\tfrac{1}{2}k_y a)\sin(\tfrac{1}{2}k_z a),
\end{aligned}
\tag{16}
$$

where a is the lattice constant and E_p and γ's are the parameters of the tight binding model. First row (column) of the matrix correspond to s-orbital, second p_x-orbital, third p_y-orbital and fourth p_z-orbital. Due to the symmetry there will be only six parameters, one of which gives the energy scale. The parameters are chosen so that the energy bands for the three main crystal directions (111), (110) and (100) (ΓL, ΓK and ΓX, respectively) are free electron like up to the Fermi energy. In practice this is done by minimizing the mean square deviation of the calculated energy bands from the free electron parabola at the three directions between 0 and k_F. Due to the numerous local minima in the space of six parameters it was necessary to use a Monte Carlo optimization method. The corresponding band structure is shown in Fig. 9 together with the free electron band.

The matrix elements in Eq. (16) have been obtained by summing over

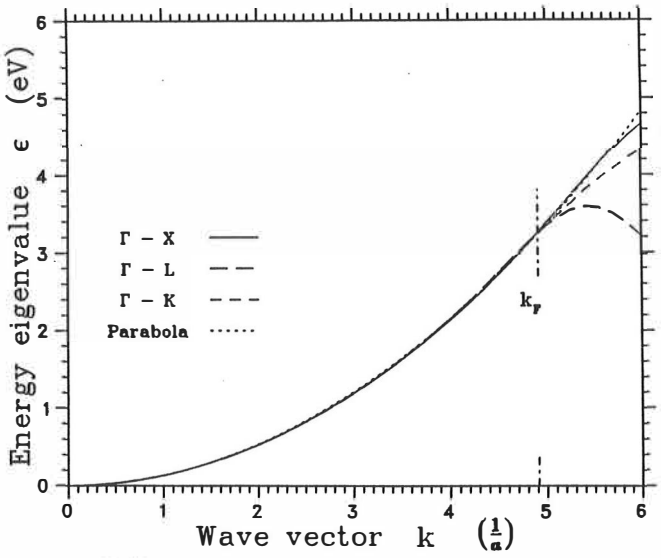

Fig. 9. Tight binding band structure for an fcc lattice. The lowest energy band (s-electron) has been fitted to the free electron parabola. k is in a units of $1/a$.

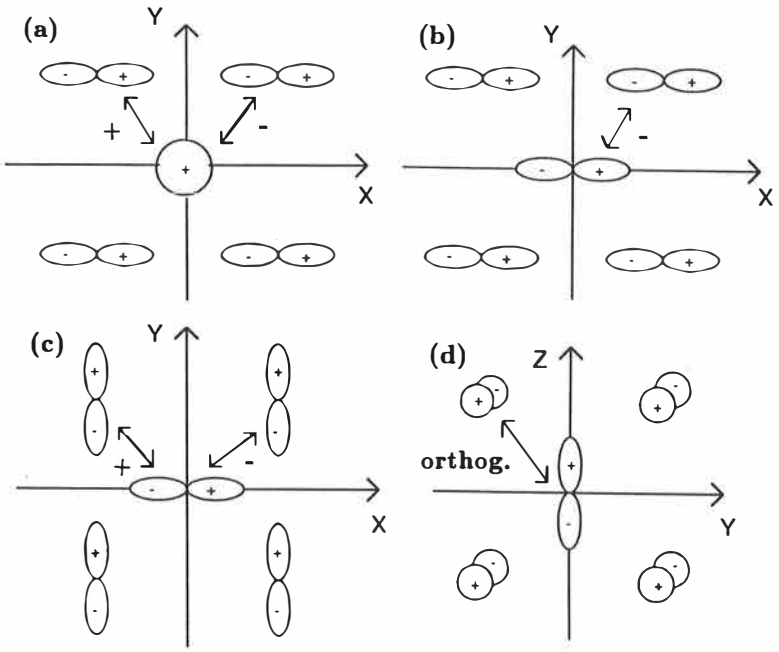

Fig. 10. **a)** sp_x-interaction, parity changes in x-direction. **b)** p_xp_x-interaction, parity does not change. **c)** p_xp_y-interaction, parity changes in both direction. **d)** p_zp_x-interaction, the orbitals are orthogonal.

the contributions of the nearest neighbours. The parity between the neighbouring orbitals determine the contribution as follows (see Fig. 10):

$$H_{ij} \propto \begin{cases} \cos\frac{1}{2}k_x a \cos\frac{1}{2}k_y a & \text{, if parity does not change,} \\ i\cos\frac{1}{2}k_x a \sin\frac{1}{2}k_y a & \text{, if parity changes in y-direction,} \\ i\sin\frac{1}{2}k_x a \cos\frac{1}{2}k_y a & \text{, if parity changes in x-direction,} \\ -\sin\frac{1}{2}k_x a \sin\frac{1}{2}k_y a & \text{, if parity changes in both direction.} \end{cases} \tag{17}$$

The arrows in Fig. 10 present the interaction between the orbitals (all arrows have not been drawn) and the sign beside the arrow is the parity. The interaction between the orthogonal orbitals is zero. Figure 10 present 2-dimensional planes cut from the 3-dimensional structure. Fig. 10a shows p_x-orbitals around the s-orbital. The parity changes in the x-direction, because of the sign of the interaction between orbitals changes. The parity does not change in the y-direction. The change of parity is examined in all three planes (xy, yz, zx) for matrix element H_{ij} and the corresponding element is taken from Eq. (17). There is interaction between p_x-orbitals in Fig. 10b. The interaction between every orbital is negative and therefore the parity does not change.

The rules of Eq. (17) can now be used to determine the matrix for a cluster. The matrix elements will be denoted by $H_{ij\alpha\beta}$ where i and j denote the atoms and α and β the orbitals (s, p_x, p_y, p_z). In all cases i and j are the nearest neihgbours. In the case of an fcc cluster we will have the following nonzero matrix elements:

$$\begin{aligned}
H_{iip_np_n} &= E_p, \\
H_{ijss} &= \gamma_0/4, \\
H_{ijp_np_n} &= \begin{cases} \gamma_1/4, & \text{if } R_n = 0, \\ \gamma_2/4, & \text{otherwise,} \end{cases} \\
H_{ijp_xp_y} = H_{ijp_yp_x} &= \begin{cases} \gamma_4/4, & \text{if } R_xR_y>0, \\ -\gamma_4/4, & \text{if } R_xR_y<0, \end{cases} \\
H_{ijp_yp_z} = H_{ijp_zp_y} &= \begin{cases} \gamma_4/4, & \text{if } R_yR_z>0, \\ -\gamma_4/4, & \text{if } R_yR_z<0, \end{cases} \\
H_{ijp_xp_z} = H_{ijp_zp_x} &= \begin{cases} \gamma_4/4, & \text{if } R_zR_x>0, \\ -\gamma_4/4, & \text{if } R_zR_x<0, \end{cases} \\
H_{ijsp_n} = -H_{ijp_ns} &= \begin{cases} \gamma_3/4, & \text{if } R_n>0, \\ -\gamma_3/4, & \text{if } R_n<0, \\ 0, & \text{if } R_n = 0, \end{cases}
\end{aligned} \tag{18}$$

where n refers to the x-, y- or z-component and $R = R_i - R_j$ is the vector between the lattice sites i and j.

3.3. Lattice-gas Monte Carlo

An ensemble of clusters with a fixed number of atoms and a given temperature, is obtained using a Monte Carlo method with Metropolis algorithm[57]. The starting geometry is chosen to be a sphere and the atoms are bound to be in the fcc lattice sites. In each Monte Carlo step one atom is moved from the cluster into an empty lattice site which can be either inside the cluster or on its surface. Evaporation of atoms or dissosiation of the cluster is not allowed. However, the clusters were allowed to have vacancies and overhangs. The total energy has to be calculated a few million times in order to get a good statistics. Thus, we need a fast method to estimate the total energy.

Ab initio calculations and the effective medium theory[58] has shown that a good estimate for the total energy is obtained by calculating the number of nearest neighbours for each atom

$$E_{\mathrm{tot}} = \sum_{j}^{N} -E_{\mathrm{c}}\sqrt{C_j/C_{\mathrm{b}}}, \tag{19}$$

where E_{c} is the cohesive energy, C_j is the coordination number for atom j and C_{b} the coordination number in the bulk (12 for the fcc structure). It has been proved[49] that the total energy in the Hückel model depends principally on the coordination number for atoms. The "exact" total energy can be calculated as a sum over of occupied single electron eigenvalues. The approximative total energy corresponds to the "exact" total energy very well. It can be used to determine the ground state geometries of the lattice gas clusters. However, the approximative scheme is not applicable in very small clusters where the electronic shell structure has to be taken into account[59].

In the lattice gas model the melting transition of the clusters is not defined.

On the other hand, the lattice gas surface has a roughening transition[60]. The estimated roughening transition of (111) surface with the square root potential, Eq. (19), is about 0.65 E_c [61]. Using the cohesive energy of sodium, the temperature for the roughening transition is about 850 K. This is well above the melting temperature of sodium (371 K). This apparent discrepancy is a basic property of the lattice gas model[62].

The probability to move an atom in the Metropolis Monte Carlo simulation is strongly temperature dependent. The ground state geometries can be found by low temperature simulations. The ground state geometries consist basically of (111) surfaces. Small facets of (100) surfaces cut off the sharp corners. The ground state structures resemble Wulff polyhedra which correspond to the ground state geometry of an infinite cluster[41]. In the finite clusters the minimization of the surface energy gives slightly different structures and the actual shape depends on the number of atoms in the cluster. Examples of ground state clusters are shown at first column in Fig. 11. The ground state structures are far from spherical. This means that the electronic shell structure is not seen in these clusters.

In the finite temperature studies we used ensembles with thousand clusters in each. Three cluster sizes were studied, 55, 138 and 249. The 55 and 249 clusters can be formed by taking closed spherical shells around the center atom. The number of atoms in 138 cluster correspond to the electron magic number. The most spherical structures are in the second column and the other columns show examples of the random clusters formed by Monte Carlo method. The 55 atom clusters have more indefinite forms than the 249 atom clusters. This is due to the variation of total energy per atom. The variation in the small clusters is bigger than on the big clusters because of the number of atoms.

3.4. Shell structure in the sp-model

The shell structure for the simple Hückel model corresponded to the free electron model only in the low energy states well below the Fermi energy. The

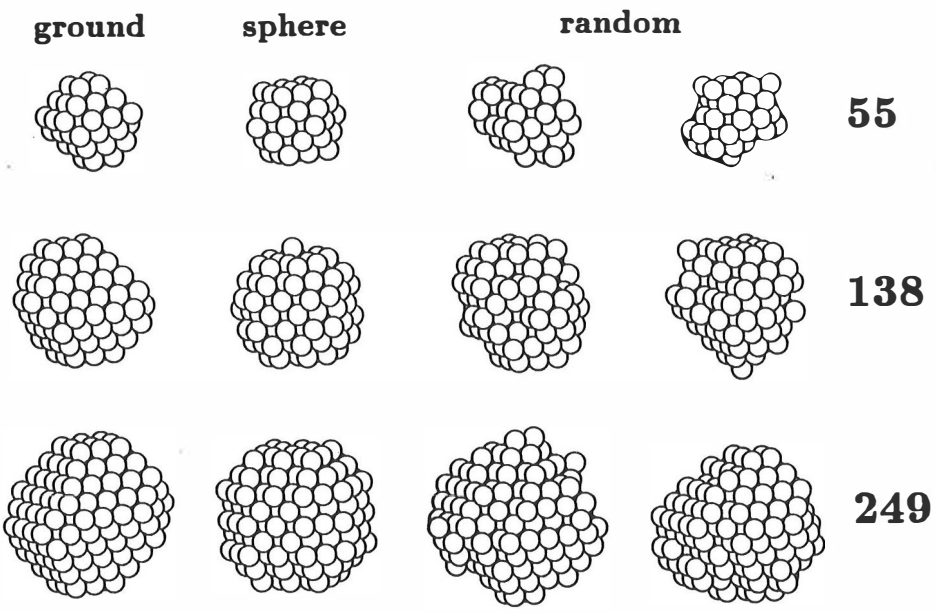

Fig. 11. Examples of cluster geometries for 55, 138 and 249 atom clusters. From left to the right are the ground state geometry, the most spherical geometry and two random geometries from the Monte Carlo calculation, respectively.

improvement for the shell structure which have been brought about by sp-model is seen in Fig. 12. The shell structures have been calculated for an fcc cluster of 249 atoms using different models. The discrete levels have been smoothened with a Lorenzian (from Eq. 7). A value 0.025 eV have been chosen for Γ (this width does not have any physical meaning). Figure 12a shows the density of states of the sp-Hückel model. The shell structure is seen more clearly at high energies than in the simple Hückel model, shown in Fig. 12b. Also the increase in the average density of states below the Fermi level, seen in 12b, is removed with the sp-model. Figure 12c gives the density of states in a spherical box with the radius of a 249 atom sodium cluster. Figure 12d shows the density of states for the ground state geometry. The ground state geometry is strongly faceted. This is known to destroy the shell structure, as shown in Section 2. It is clear that the shell structure typical to a spherical cluster has completely vanished, in Fig. 12d.

The sp-model does not show the shell structure of the free electron sphere all the way up to the Fermi energy. The reason for this is the roughness of the cluster

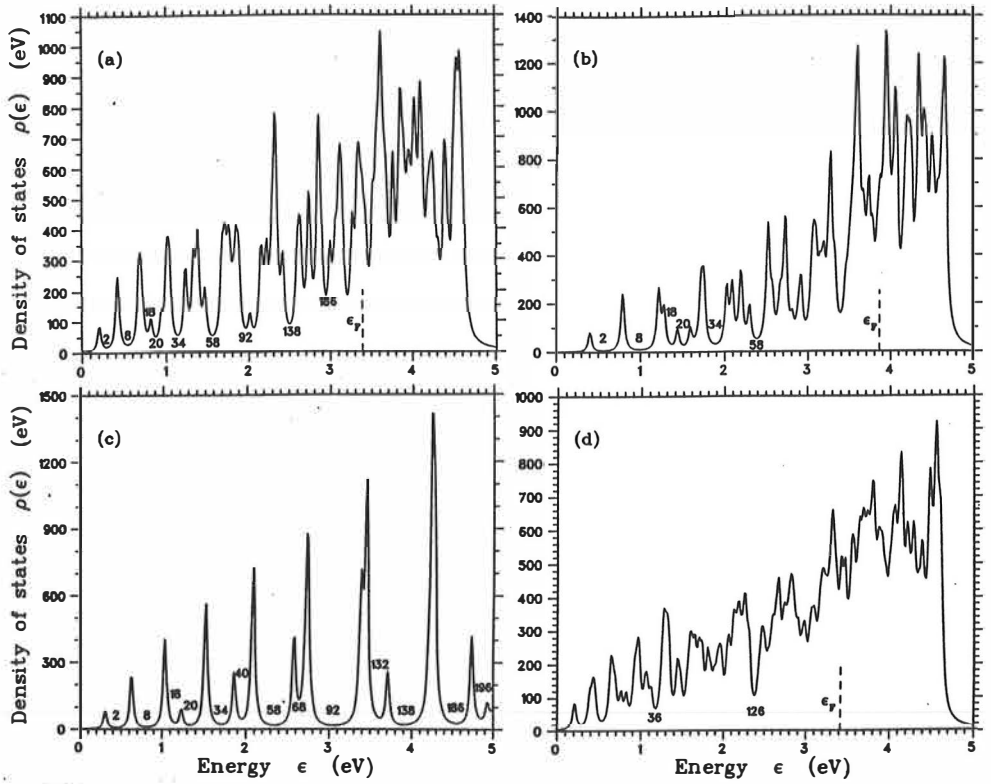

Fig. 12. Density of states in a 249 atom sodium cluster: **a)** sp-Hückel model for a spherical fcc cluster, **b)** simple Hückel model for a spherical fcc cluster, **c)** free electron sphere, **d)** the ground state cluster.

surface. Even the most spherical fcc cluster seems to have so rough surface that the energy gaps related to the shell structure disappear at the Fermi level. This gives more confidence to the suggestions that the large clusters, where the shell structure has been observed, do not have the lattice structure of the bulk metal.

We now proceed to study the clusters at finite temperatures. In order to get an ensemble of clusters with different geometries we have used a temperature of 800 K in simulations (at 400 K the cluster remains mainly in its ground state). Each cluster with a different surface shape has a different electronic structure. The main differencies occur close to the Fermi level. Figure 13a shows the density of states for 5 clusters chosen arbitrarily from the ensemble of 970 clusters. The density of states is very similar in each cluster only upto about 1.5 eV where the minimum corresponds to the shell closing 58. At larger energies the shell structure differs

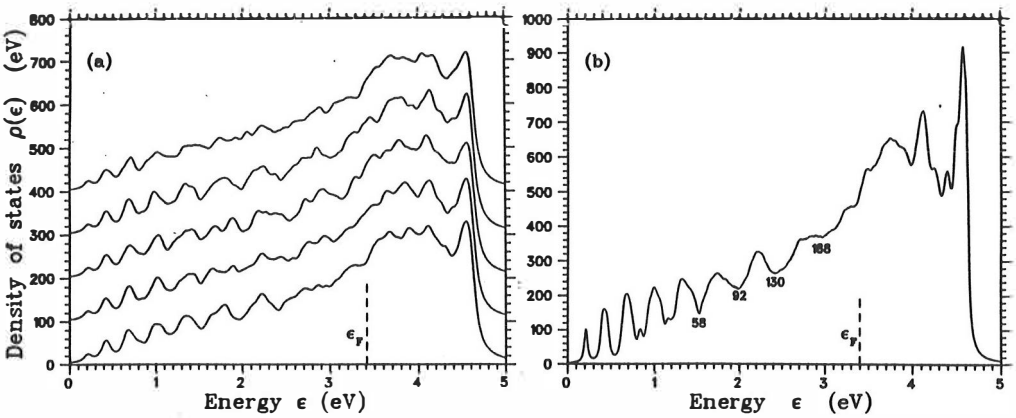

Fig. 13. **a)** Density of states for five random clusters. **b)** The average density of states for the ensemble of 970 clusters of 249 atoms. The discrete eigenvalues have been convoluted with a Lorenzians with the width of **a)** 0.3 eV and **b)** 0.025 eV.

from cluster to cluster. Figure 13b shows the average density of states for the whole ensemble of 970 clusters at 800 K. The average shell structure shows clear minima still at the free electron shell closings (Fig. 12c) 92, 138 and 186 (the actual minima indicated at the figure are 92, 130 and 188 but the small deviations could be due to the insufficient statistics). It is important to notice that the average density of states shows the shell structure at as high energies as the most spherical cluster in the lattice gas model.

3.5. Level spacing statistics

At a finite temperature the electronic properties of the clusters depend on the distribution of energy levels near the Fermi level. The geometry of the cluster has an effect on the distance between neighbouring levels. In case of an infinite free electron metal the average level spacing around the Fermi level is

$$\Delta = \frac{4\epsilon_F}{3N}, \tag{20}$$

where N is the number of electrons. We have studied the level spacing distribution

for the fcc lattice gas clusters formed by Monte Carlo method. The electronic structure is calculated using the sp-Hückel model. The level spacing distribution has only been determined close to the Fermi level (six level spacings around the Fermi level). From the 1000 clusters we have then obtained 6000 level spacings which is enough to determine the distribution.

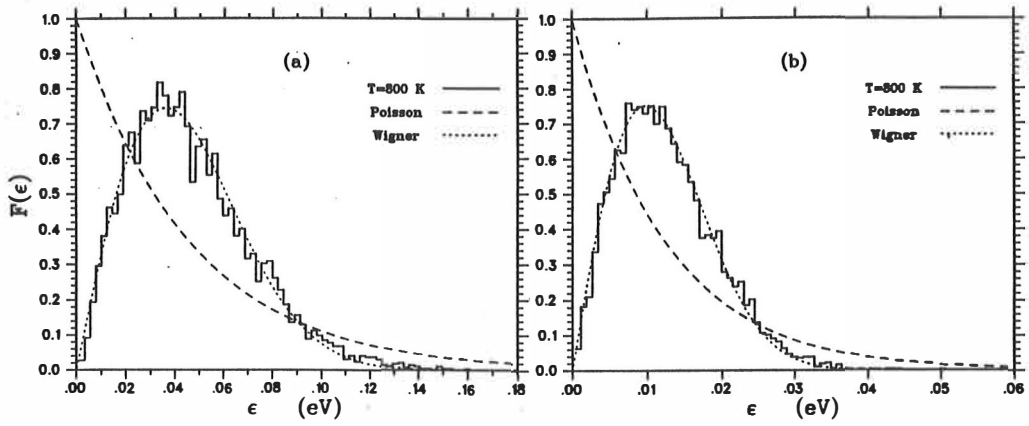

Fig. 14. Level spacing distribution for the clusters generated using the Monte Carlo method. **a)** 55 atom clusters at 800 K and **b)** 249 atom clusters at 800 K. The Poisson and Wigner distributions are shown for comparison.

Figure 14 shows the level spacing distribution for two sizes of clusters (55 and 249). The Poisson distribution (the dashed lines)

$$P(\epsilon) = A \exp(-\epsilon/\epsilon_{\mathrm{ave}}) \tag{21}$$

and the Wigner distribution (the dotted lines)

$$P(\epsilon) = B\epsilon \exp(-\epsilon^2/4\pi\epsilon_{\mathrm{ave}}^2) \tag{22}$$

have been drawn for comparison. A and B are the normalization constants and ϵ_{ave} is the average level space. It is clear that in both cases the distribution fits to the Wigner distribution.

In nuclear physics context the level spacing distribution is usually analyzed using the random matrix theory[56], which is shown to give the Wigner distribution. The elements of a random matrix are random numbers with a Gaussian distribution. In the simple Hückel model the matrix elements are either 1 or 0 depending whether the corresponding atoms are nearest neighbours or not, respectively. In sp-model the matrix elements can have seven different values. These kind of 'random matrices' seem also to produce a Wigner distribution for the large eigenvalues[63]. Small eigenvalues show the shell structure and the Poisson distribution. This may be due to the fact that only the matrix elements corresponding to the surface atoms are 'random'.

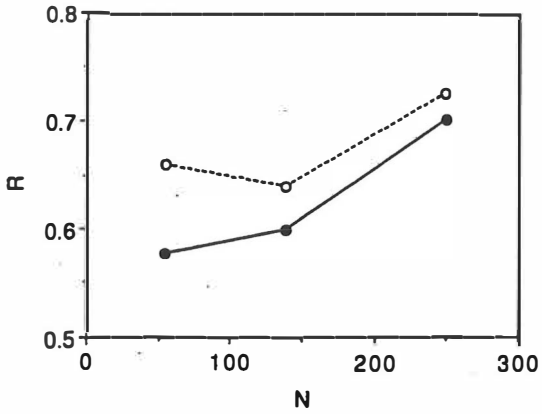

Fig. 15. Width of the level spacing distribution ($R = 3\Delta N/4\epsilon_F$) as a function of the cluster size. The black dots are the average level spacing determined using seven levels close to the Fermi level and the open circles are estimates for the level spacings at the Fermi level.

Bucher et al.[64] have studied the level spacing statistics with a model closely related to ours. They have used the simple Hückel model and generated the cluster geometries by evaporating atoms from a cubo-octahedron. Their results show that the distribution in the middle of the band is a Wigner distribution which becomes narrower when the temperature rises. Tanaka and Sugano[65] have simulated the level statistics in two and three dimensional tight binding models and studied the relation of the tight binding model to the random matrix theory[63]. They found out that the distribution could be fitted with a Brody distribution which approaches to

the Wigner distribution when the roughness increases. Ratcliff[66] has studied the level spacing distribution using free electrons confined by irregular hard walls. The study is limited only to a single large angular momentum state, but the resulting distribution is again a Wigner distribution.

Figure 15 shows the average width of the level spacing distribution as a function of the cluster size. The width increases towards the bulk-value Δ from Eq. (20). The average level spacing increases with the size of the cluster. The increase of the temperature roughens the surface and also makes the average level spacing narrower. The average level spacing is nearer the bulk-value in random spherical clusters than in the Monte Carlo clusters. The physical interpretation is that less spherical clusters have narrower energy bands and thus smaller average level spacing.

The Monte Carlo method used to produce the cluster ensembles neglected all shell structure effects. In reality the clusters having a larger energy gap just at the Fermi level would have a reduced total energy (the levels below the Fermi level would be pushed down). This could appear in the level spacing distribution as a slightly larger energy gap just at the Fermi level than the neighbouring gaps. To mimic this effect we have calculated the total energy of cluster ensembles also summing exactly the one electron energy eigenvalues. These clusters whose 'exact' total energy is below the approximative total energy of Eq. (19) have a clearly larger average gap at the Fermi level as seen in Fig. 15. The opening of a larger gap at the Fermi level is clearly seen at the zero temperature calculations[59].

4. Shell structure in large nonspherical metal clusters

4.1. Theoretical model

The effects of the geometry of a cluster on the shell structure have been studied already in paragraph 2.4. There it was shown that the surface faceting of the fcc cluster can destroy the electronic shell structure when the cluster has about 100 electrons. Recently, a set of magic numbers for large simple metal clusters have

been observed[3,8,12]. These correspond to the geometrical packing of atoms in an icosahedral structure. In the case of sodium clusters the magic numbers between 1500 – 3000 atoms can be determined either by the electronic structure[4] or by the geometry[2] depending upon the experimental conditions.

The Hückel model used in Sect. 2 corresponds to a potential box with hard walls and it can be used only for a cubic structure. Here we want to develope a model which is as good for icosahedral as for cubic clusters. For large sodium clusters, the effective potential of the electron inside the cluster is nearly constant. A reasonable approximation for the effective potential is then a finite potential well with a depth determined by

$$V_0 = -\phi - \epsilon_F, \tag{23}$$

where ϕ is the work function of the metal and ϵ_F the Fermi energy measured from the bottom of the conduction band. For spherical clusters, the radius is determined by $r_0 = N^{1/3} r_s$, where N is the number of atoms in the cluster and r_s the Wigner-Seitz radius.

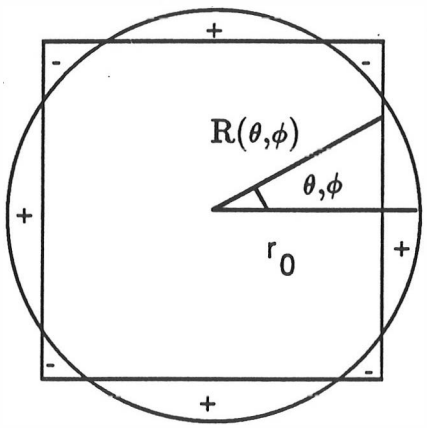

Fig. 16. The difference between geometries of spherical and nonspherical clusters (perturbation potential). The difference between potentials is restricted within a narrow region close to the cluster surface (marked with + or −). The sign is the sign of perturbation potential. r_0 is the radius of spherical cluster and $R(\theta, \phi)$ is the angle-dependent distance defined as the distance from the center of the cluster to its surface.

The nonspherical clusters are described by using nonspherical potential wells

with the same depth, Eq. (23), and volume as the spherical cluster. The finite potential well can be changed to the wanted geometry by adding a perturbation potential $\Delta V(\mathbf{r})$, which is defined as the difference between the potentials of spherical and nonspherical clusters as follows:

$$\Delta V(\mathbf{r}) = V_0\{\theta[R(\theta,\phi) - r] - \theta(r_0 - r)\} \tag{24}$$

where θ is the step function. We can see from Figure 16 that the difference between the spherical and nonspherical potentials is restricted within a narrow region close to the cluster surface. If the surface of the nonspherical cluster is closer (further) to the center of the cluster than the surface of spherical cluster, the perturbation potential has a positive (negative) value.

In order to calculate the electron levels for nonspherical case we start from the solution of the Schrödinger equation for the spherical geometry,

$$\psi_{nlm}(\mathbf{r}) = R_{nl}(r)Y_{lm}(\theta,\phi), \tag{25}$$

where $Y_{lm}(\theta,\phi)$ are the spherical harmonics. The radial wave function $R_{nl}(r)$ and the corresponding energy eigenvalue are obtained numerically. The energy eigenvalues for the nonspherical potential well can be obtained by diagonalizing the Hamiltonian matrix

$$\langle nlm|H_0 + \Delta V|n'l'm'\rangle, \tag{26}$$

where H_0 is the single-particle Hamiltonian for the spherical potential well. Because the perturbation potential of Eq. (24) is nonzero only close to the radius r_0, it is convenient to expand the radial wave function as

$$R_{nl}(r) = R_{nl}(r_0) + R'_{nl}(r_0)(r - r_0), \tag{27}$$

where R'_{nl} is the derivative of R_{nl}. The integration over the distance r in Eq. (26) can then be done analytically.

4.2. Shell structure in icosahedral and cubo-octahedral clusters

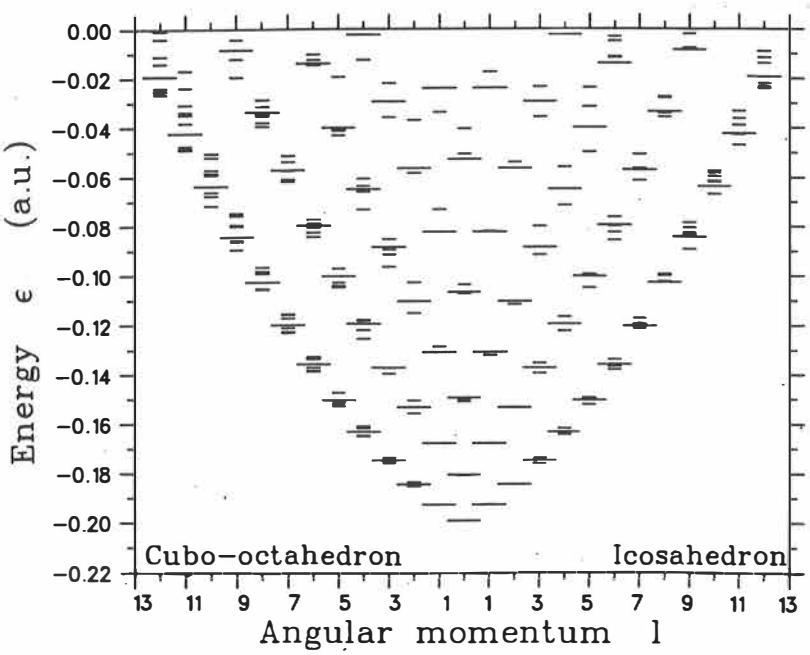

Fig. 17. Level structure of a 309-atom sodium cluster approximated with a square-well potential. For the nonspherical clusters the angular momentum is only approximately correct. The long lines represent the levels of the spherical well. The short lines on the left-hand side represent the levels of the cubo-octahedral well, and those on the right-hand side represent the levels of the icosahedral well.

The energy eigenvalues for the nonspherical geometry are formed by diagonalizing the matrix of Eq. (26). The wave function for each energy eigenvalue are also obtained from the diagonalisation. The wave function has as many components as the dimension of the matrix, and n, l and m are not any more good quantum numbers. However, if the perturbation is weak one of the expansion coefficients is much larger than the others and we can associate n, l and m numbers also to the perturbed states. Thus, the energy eigenvalues can be labelled according to the quantum numbers as seen in Figure 17. The level mixing is small for the small clusters but with the increasing cluster size the mixing becomes more important, and thus the labelling of the energy eigenvalues becomes more difficult.

Figure 17 shows the electronic shell structures for spherical, icosahedral and cubo-octahedral potential wells corresponding to clusters with 309 atoms. The degeneracy of each level is $2l + 1$ (plus the spin degeneracy) in the spherical case but the levels split in the nonspherical case, since the maximum degeneracy in the cubic (cubo-octahedral) symmetry group is three and in the icosahedral one it is five. In the case of the icosahedral cluster the splitting of nl-levels remains smaller than the energy difference between the different l-shells, whereas for the cubo-octahedron the splitting is about the same magnitude as the difference between the shells. Therefore, the icosahedral 309-atom cluster will have the main shell structure closely similar to that of the spherical cluster.

It is quite difficult to see the overall shell structure from Fig. 17. Therefore, it is more illustrative to plot the density of states according to Eq. (7). The value of the width $\Gamma = 0.001$ a.u. The electronic structure of complete icosahedral and cubo-octahedral sodium clusters have been calculated between $147 \leq N \leq 1415$. The energy eigenvalues for 147- and 309-atom clusters have been calculated by including all bound basis states of the spherical potential well in the Hamiltonian matrix. For larger clusters the number of nlm-basis functions have been restricted to be about 450.

Figure 18 shows the densities of states for the 309- and 923-atom icosahedral and cubo-octahedral sodium clusters. In each figure, the density of states of a spherical cluster with the same size is shown with a dashed line. The selection of the size of the cluster has been done on the grounds that the outermost shell is closed. The Fermi level changes from about –0.08 to –0.07 a.u. when the cluster size increases from 309 to 1415 atoms. We can see from Fig. 18a that the magic numbers are the same for the icosahedron and for the sphere still above the Fermi level. However, we notice that in details the subshell behaviour in the two cases is different. For the cubo-octahedron in Fig. 18b, only the lowest energy levels are the same as for the sphere. The situation is similar both in 147-atom cluster and in 309-atom cluster. The correspondence of the energy levels of the cubo-octahedron compared to sphere does not reach the Fermi level. The level structure of the smallest cubo-octahedral clusters agree with that obtained by Martins[67] using an

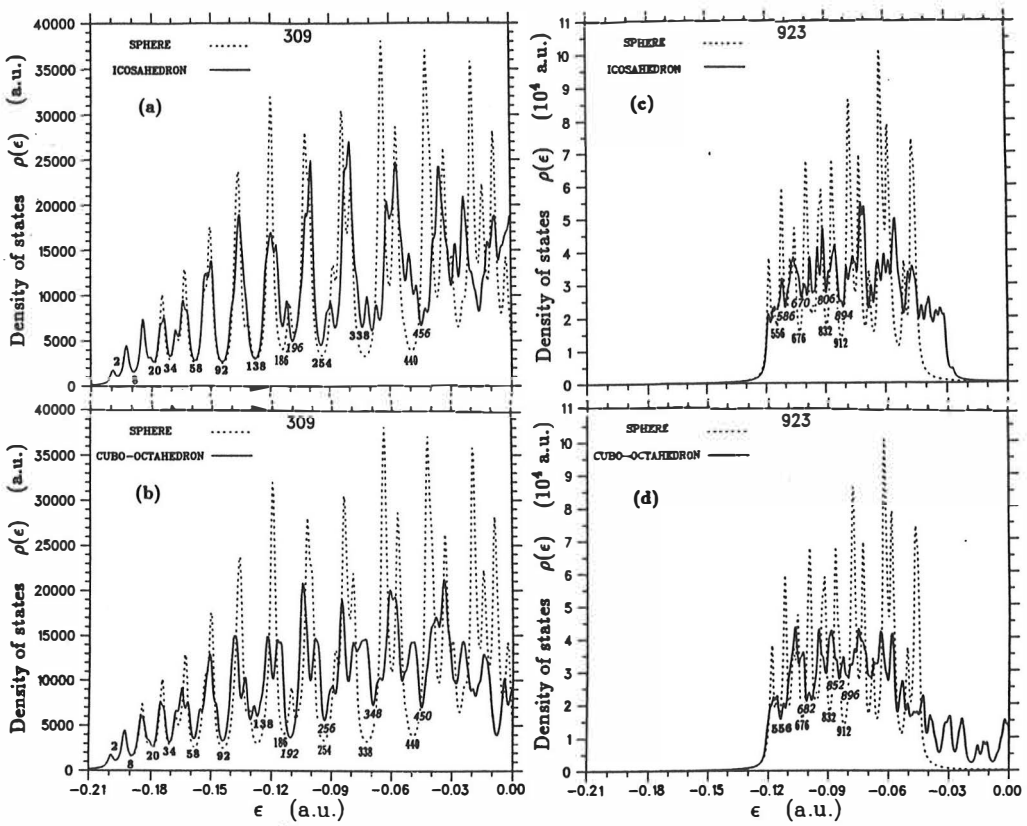

Fig. 18. Density of states of the 309- and 923-atom sodium cluster calculated for a spherical (dashed lines), (a,c) icosahedral, (b,d) cubo-octahedral square well. The numbers below the energy gaps indicate the corresponding magic numbers. Italic numbers denote the magic numbers for the icosahedral or cubo-octahedral potential. A boldface number is used when the spherical and polyhedral potential give the same magic number.

ab initio pseudopotential approach.

For clusters from 561 to 1415 atoms, the shell structure have been calculated only close to the Fermi level. From Fig. 18c we can see that up to the Fermi energy the main shell structure of the icosahedral clusters is still quite similar to that of a sphere. This is valid also in the case of a 561-atom cluster. The exact numbers corresponding to the shell fillings are different, however. It should be noted that the grouping of the levels of different angular momentum values is sensitive to the details of the spherical potential. Therefore, it is not surprising that when the spherical

potential is replaced with an icosahedral potential, the exact magic numbers can change even if the shell structure is still very similar to that of a sphere. This is clearly seen in the case of the 309-atom cluster in Fig. 18a, where the sphere gives a deeper minimum for the shell closing at 186 electrons, whereas in the case of the icosahedral cluster the competing minimum at 196 electrons is deeper. For the large (more than 561 atoms) cubo-octahedral clusters, the results of the shell structure are only approximative due to the approximation in Eq. (27). This approximation and the less spherical geometry of the cubo-octahedron than that of the icosahedron cause that the disturbation in the shell structure due to the mixing of the included levels with the excluded levels, seen in Fig. 18d, is much greater in the case of cubo-octahedral clusters than in the icosahedral ones (Fig. 18c).

4.3. Deformed liquid clusters

The large magic numbers corresponding to the electronic shell structure have been observed experimentally for warm clusters[4]. They could either be in the liquid state or have liquid-like surface. The shape of the cluster will then be different from that of a crystalline cluster. The surface tension will force the liquid clusters to be spherical but at finite temperatures there will be fluctuations at the surface structure. It is then important to know the effect of the shape oscillations to the electronic shell structure. Using the potential-well approximation such effect can be studied. The energy of the surface-wave excitation can be estimated from the liquid drop model where the cluster energy is determined from the surface and curvature energies. This model gives good average estimates for the size dependence of the total energy of jellium clusters[68]. In small clusters, there is an interplay between the shell structure and the deformation of the clusters that has been studied using spheroidal[69,70] or octupole deformations[71].

Since we are concentrating on large clusters, the shell structure effects on the deformation can be neglected. For simplicity, we assume the liquid to be incompressible. In the calculations the potential well has been taken to be a prolate spheroid. The energy associated to the deformation is estimated solely from the

increase of the surface energy (in small clusters the change in the one-electron spectrum would also be an important part of the total energy). The equipartition theorem requires that each surface mode has an energy of the order

$$E_{sw} \approx k_B T. \tag{28}$$

Defining the amplitude of the surface wave by $x = (b - r_0)/r_0$, where b is the shorter semiaxes of the spheroid, we obtain for small deformations

$$E_{sw} \propto r_0^2 x^2. \tag{29}$$

The change in the energy eigenvalues due to the deformation[72] is

$$\Delta\epsilon \propto \frac{x}{r_0}, \tag{30}$$

when $[r_0 - R(\theta, \phi)] \propto x$. Combining Eqs. (28), (29) and (30), and using the fact that $r_0 \propto N^{1/3}$, we get the following important result:

$$\Delta\epsilon \propto \frac{\sqrt{k_B T}}{N^{2/3}}. \tag{31}$$

This means that for a given temperature the effect of the surface waves on the energy levels decreases when the cluster size increases. On the other hand, for a given size the effect of the surface waves on the energy levels increases with temperature. The energy difference between the major shells in a spherical cluster is proportional to $N^{-1/3}$. The relative disturbance of the surface waves on the shell structure decreases when the cluster size increases and depends only weakly on the temperature.

Figure 19 shows the level structure of a 1415-atom cluster as a function of the degree of the deformation (b/a-ratio, a and b are the semiaxes of spheroid). Only the prolate case and the levels close to the Fermi level were considered. If the deformation decreases below 0.99, the energy levels start to cross each other.

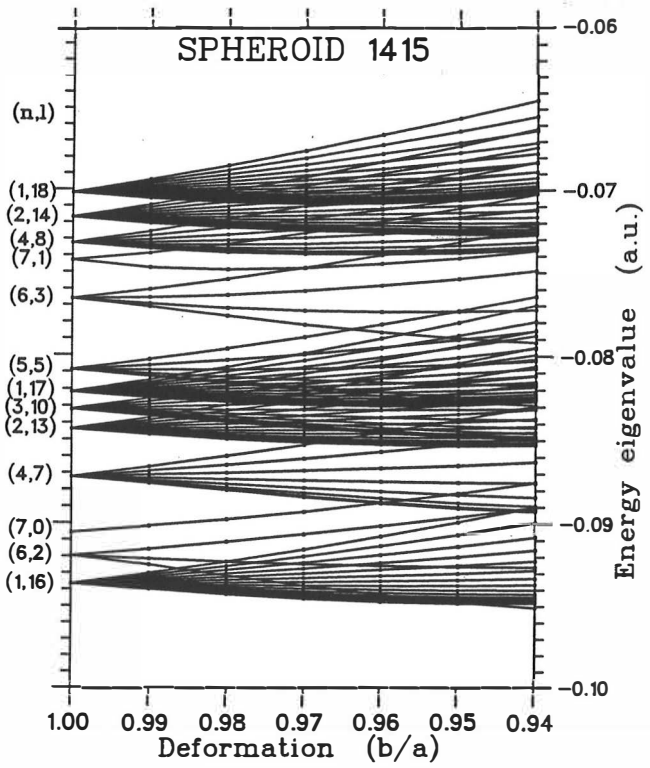

Fig. 19. Single-electron energy levels for a prolate spheroidal potential well as a function of the deformation (b/a). The numbers in parentheses show the radial and angular quantum numbers (n,l). $n = 1$ corresponds to the lowest state for each angular momentum.

Figure 20 shows the density of states for a prolate spheroid corresponding to a 309-atom sodium cluster. The densities of states are shown corresponding to an average instantaneous deformation at 800 K and for the melting temperature. The effect of the deformation is fairly small even at the higher temperature. This is true also for a 923-atom cluster. If the temperature increases or the size of the cluster decreases, the deformation of the cluster will increase. The shell closing numbers of the spheroid correspond to those of a sphere only for few lowest energy levels because of the deformation (seen in Fig. 20b).

The spheroidal deformation (quadrupole deformation) is the simplest surface-wave mode. In a real sample of clusters, many different surface modes will exist. However, the energy of any higher multipole mode estimated from the surface energy corresponds to an amplitude smaller than that of the quadrupole mode. This follows from the faster increase of the surface area for the higher multipoles. It is then

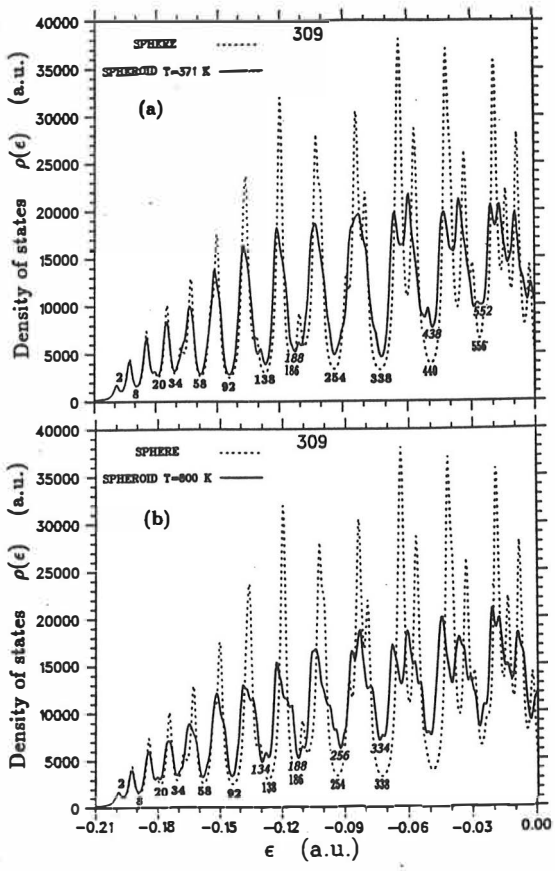

Fig. 20. Density of states of a spheroidal 309-atom sodium cluster. The deformations correspond to temperatures (a) 371 K and (b) 800 K.

expected that the quadrupole mode has the largerst effect on the shell structure of liquid clusters. The melting point and the boiling point decreases when the cluster becomes smaller. In each cluster these are lower than in bulk solid. The higher temperature considered, 800 K, is already difficult to achieve in small clusters, since they would start to evaporate atoms. We can conclude that the surface fluctuations in liquid sodium clusters do not destroy the main features of the electronic shell structure.

5. Existence of the star orbit in metal clusters

5.1. Supershell structure

The shell structure was defined as large energy gaps between the energy levels. The modulation of the shell structure is called supershell structure[25]. It is illustrated in figure 21 which shows the shell structure for free electrons in a cavity. The radius of spherical potential box corresponds to 10000-atom cluster. The energy eigenvalues have been obtained from the zeros of the Bessel functions. The density of states are given as a function of wave vector k in order to make the peaks to appear approximately equi-distant. The difference between the peaks is $\Delta k = 0.5 \times N^{-1/3}$ Å^{-1}. For each single-particle energy ϵ_{nl}, a wave vector k_{nl} is defined in atomic units as

$$k_{nl} = [2(\epsilon_{nl} - V_0)]^{1/2}. \tag{32}$$

In order to visualize the supershell structure clearly, the discrete energy levels are smoothened with a Lorenzian. In practice, this is done by adding an imaginary part k_i to each k_{nl}. The level density is given by

$$\rho(\epsilon) = 2 \sum_{n,l} \frac{2(2l+1)}{\pi} \frac{2k_i k_{nl}}{(k^2 - k_{nl}^2)^2 + (2k_i k_{nl})^2}, \tag{33}$$

where k_i is chosen to be $0.13 \times N^{-1/3}$ Å^{-1}, which is a quarter of the spacing of successive shells.

The supershell structure is clearly seen in Fig. 21. The first node is located in the place which corresponds to 1000 electrons. The shell structure which corresponds to short-wavelength periodic oscillations disappear almost completely in that place. Thus, the observation of supershells requires more than 1000 electrons. Between the nodes e.g. when $k = 0.5$ Å^{-1}, the shell structure is clearly seen. The second node locates in the place which corresponds to 3000 electrons. After that there is a weaker minimum at about 10000 electrons. The supershell effect has been observed experimentally up to 3000 electrons[4].

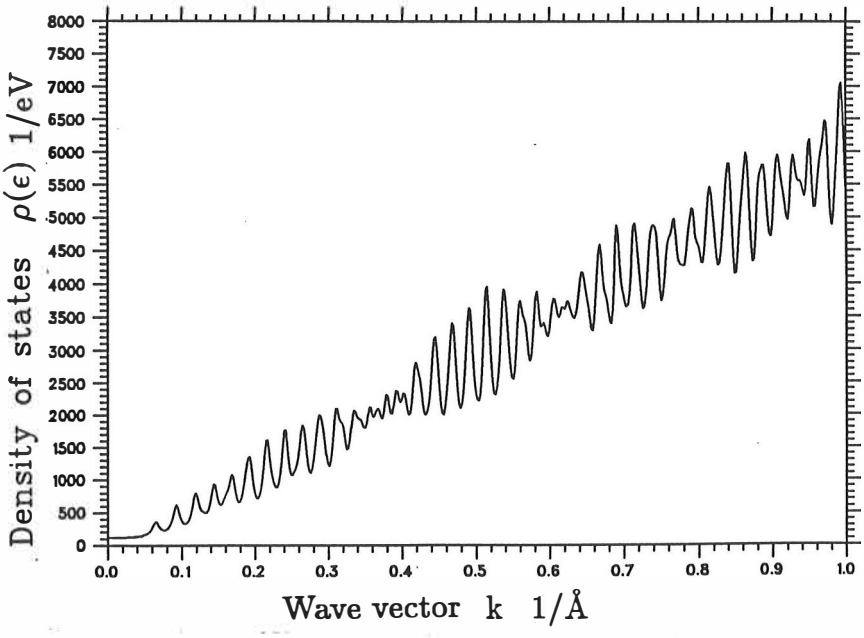

Fig. 21. The shell structure of free electrons as a function of wave vector k. The radius of the spherical potential well corresponds to a 10000-atom cluster.

It is often illustrative to use a semi-classical interpretation of the shells and the supershells. Periodic electronic shells are closely associated with a simple classical periodic orbit inside the potential. On the basis of the classical Bohr atomic model the electron orbits must have an integer number of wave lengths. In spherical potential the supershell structure is a consequence of the interference of two classical closed periodic orbits, triangular and square ones[24]. The interference is a result of the difference of the lengths of the two trajectories. The neighbouring shell spacing is proportional to the inverse of the length of the shortest orbit (triangle), while the supershell spacing is proportional to the inverse of the length difference between two orbits, which is almost 11 times the shell spacing.

Figure 22 shows a triangular orbit inside the sphere. It consists of the three changes of direction of an electron at each whole turn around the sphere. The length of the orbit between each change of direction is marked by quantum number n and the length of an orbit between each turn is marked by quantum number l. If half of the length of n is marked by m, then $n = 2m$ and $l = 6m$. The difference between lengths is obtained by adding one unit to the length of m. Thus, we have

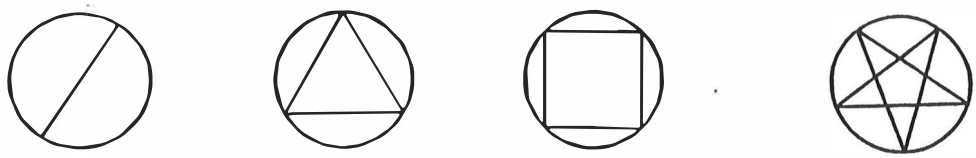

Fig. 22. Most important classical closed orbits in a spherical potential. The ratio of the radial to angular oscillations is shown in each case.

$n_1 = 2m + 2$, $l_1 = 6m + 6$, $\Delta n = n_1 - n = 2$ and $\Delta l = l_1 - l = 6$. The relation of the difference of the quantum numbers $\Delta n : \Delta l = 1 : 3$ for the triangular orbit. The five-point star orbit, seen in Fig. 22, consist of five changes of direction of the electron at two turns. Thus $n = 2m$ and $l = 10m$ for two turns and we can take $l = 5m$ for one turn. Therefore, the relation is $\Delta n : \Delta l = 2 : 5$. In a energy level structure the classical orbits can be observed from the differences of quantum numbers (Δn and Δl) between two near and successive energy levels.

In a spherical potential the energy levels have a degeneracy determined by magnetic quantum number m. The degeneracy is $2(2l + 1)$ (including spin degeneracy). With the total number N of the constituent particles the amount of degeneracy is of the order $N^{1/3}$. All states with the same $n + l$ $(2n + l)$ are completely degenerate in the Coulomb (harmonic-oscillator) potential. This additional degeneracy gives the total degeneracy proportional to $N^{2/3}$. In a square well potential the additional degeneracy is smaller and the total degeneracy will be proportional to $N^{1/2}$[73]. The wave number difference δk between neighbouring shells in Fig. 21 is approximately

$$\delta k \simeq r_s^{-1} N^{-1/3}, \tag{34}$$

where r_s is the Wigner-Seitz radius and N the number of electrons. The corresponding energy difference $\delta\epsilon$ at the Fermi level is then

$$\delta\epsilon = k_F \delta k \simeq \epsilon_F N^{-1/3} \tag{35}$$

where k_F is the Fermi wave vector and ϵ_F the Fermi energy. The total number of states in the energy range $\delta\epsilon$ at the Fermi level is $N \times \delta\epsilon/\epsilon_F = N^{2/3}$. Since in the square well the number of states in each shell is of the order $N^{1/2}$, the relative strength of the shells to the background level density is of the order $N^{1/2}/N^{2/3} = N^{-1/6}$.

5.2. Electron orbits in the Woods-Saxon potential for Al clusters

Recent experiments revealed[5,7] that the shells in Al clusters are twice denser with respect to the electron number than in alkali-metal clusters. Lerme et al.[5,6] suggested that mass spectra of Al clusters could be explained from a semi-classical picture that a five-point star orbit plays a dominant role in the shell structure. They argue that a particle moving classically cannot make a sharp turn from a soft wall unless it collides almost perpendicularly. This condition excludes the existence of the triangular and the square orbits in a suitably soft potential. The experimental evidence of the star orbit is, however, not strong. Martin et al.[7] has shown that the observed shell structure of the Al clusters could be explained from geometrical packing of ions in octahedra. Their explanation is similar to the case of large ($N > 1000$) Na clusters produced at low temperature, where icosahedral packing of ions determine the shell structure. The idea of Lerme et al. on the effect of five-point star orbit is, however, interesting enough to pursue further. Although it may not be the origin of the shell structure of Al clusters, the five-point star orbit might be important in other systems.

The potential of a spherical metal cluster is simulated with the Woods-Saxon potential

$$V(r) = -\frac{V_0}{1 + e^{\alpha(r-r_0)}}, \tag{36}$$

where V_0 is the depth of the potential well, r_0 the radius of the potential and α a parameter determining the potential softness. For making a connection to real metals we choose V_0 to be the sum of the Fermi energy (measured from the bottom of the conduction band) and the work function. The radius of the potential is

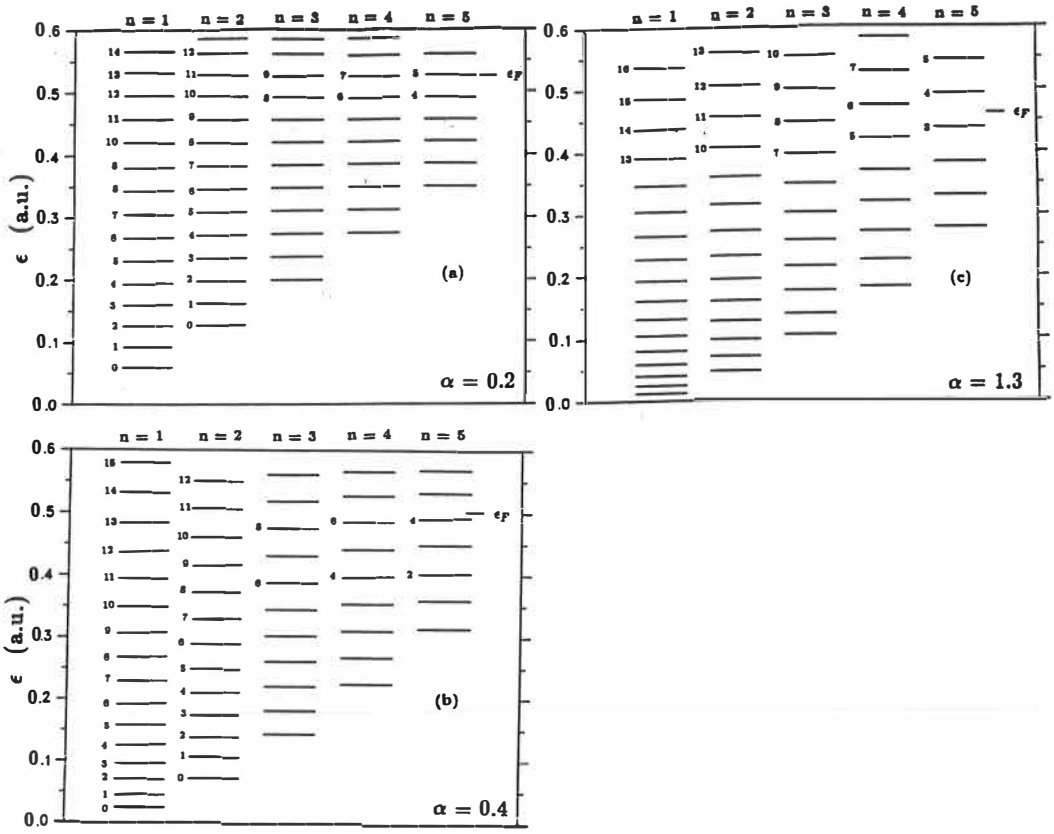

Fig. 23. Electron energy levels for three different values of α. The radius and the depth of the potential correspond to a 1000 electron Al cluster.

chosen to be $r_0 = r_s N^{1/3}$, r_s being the electron density parameter and N the number of electrons in the cluster. The calculations have been made in the potential which depth and the radius correspond to Al cluster with 1000 valence electrons. With three different values of the softness parameter α the Woods-Saxon potential corresponds to a harmonic potential, a soft potential and a hard potential well.

The level structures for Al clusters for three α-values are shown in Fig. 23 in separate columns for different n-values. For $\alpha = 0.2$ (Figure 23a) degenerate levels have the ratios $\Delta n : \Delta l = 1 : 2$, which correspond to the pendulum orbit in Fig. 22. Increase of the α lifts the levels with $n \geq 2$ up leaving the levels with $n = 1$ unchanged. At $\alpha = 0.4$ (Figure 23b) the levels of $n = 3$ are nearly degenerate to those of $n = 1$ with the angular-momentum difference $\Delta l = 5$ corresponding to the classical five-point star orbit. It should be noted, however, that the degeneracy

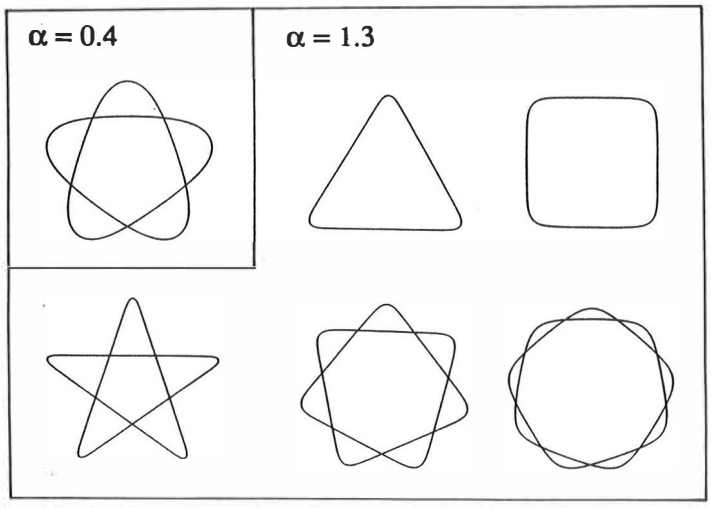

Fig. 24. Classical closed orbits at the Fermi energy (–0.15 a.u.) for Woods-Saxon potentials corresponding to 1000 electron Al clusters. All orbits with less than two turns around the center are shown (except the pendulum and the sphere).

at higher n-values is not very good. Levels with $n = 2$ lie in the middle of two neighbouring levels with $n = 1$. A further increase of α pushes the $n = 2$ levels up. They become eventually degenerate with the $n = 1$ levels with the ratio $\Delta n : \Delta l = 1 : 3$ and then go up further to be degenerate to the levels with the ratio 1 : 4. This competition of the degeneracies with the two different ratios (1 : 3 and 1 : 4) is the quantum-mechanical origin of the supershell structure. The clusters with $N = 1000$ are indeed in the nodal region of the supershell structure for Al.

The classical closed orbits have been derived numerically for different values of α. The value $\alpha = 0.2$ gives only ellipse-type orbits in accordance with a perfect harmonic oscillator. The simplest classical orbit for $\alpha = 0.4$ is the five-point star, shown in Figure 24. The hard wall potential, $\alpha = 1.3$, gives also the triangle and square orbits in addition to several star orbits. Note that the five-point star has much softer corners in the case of $\alpha = 0.4$ than in the case of $\alpha = 1.3$.

At the moment the density of states cannot be investigated experimentally expect for the Fermi energy region. The shell structure of the Al clusters have been observed in the mass spectrum after near-threshold ionization of the cluster beam, thus only at the Fermi level. Therefore, the energy difference between the lowest

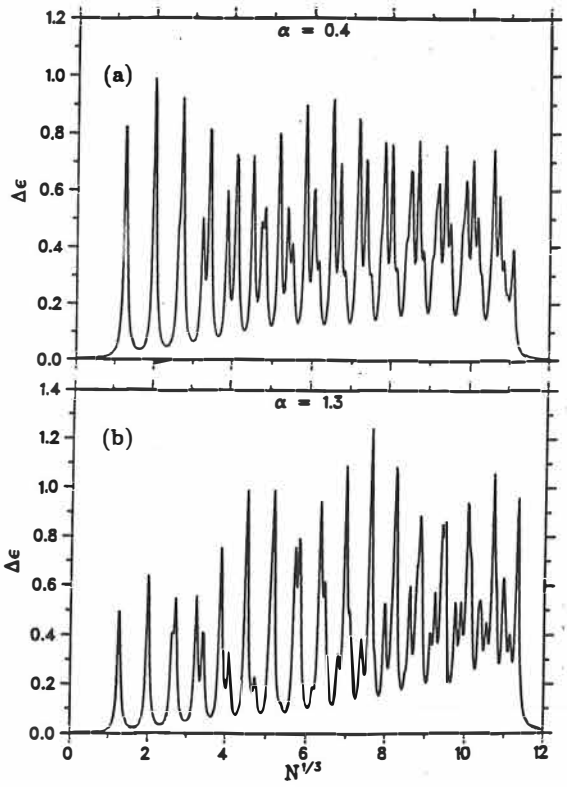

Fig. 25. The difference between the lowest unoccupied and the highest occupied energy level as a function of $N^{1/3}$, where N is the number of electrons in the cluster.
unoccupied and the highest occupied levels is calculated for each N.

$$\Delta\epsilon(N) = \epsilon_{N+1} - \epsilon_N. \tag{37}$$

To make the calculation simple the potential is fixed with the radius parameter at $N = 1000$, and electrons are put in up to each size of the cluster. The $\Delta\epsilon(N)$ have been plotted as a function of $N^{1/3}$ in Fig. 25 for $\alpha = 0.4$ and 1.3. The discrete levels have been convoluted with a Lorenzian from Eq. (7) ($\Gamma = 0.048$). When the $\Delta\epsilon(N)$ is large the ionization potential is expected to be large, and therefore the magic numbers should be observed. Peaks are equi-distantly placed in the $\alpha = 1.3$ and for $\alpha = 0.4$ each peak is divided into two peaks except for the first three. It will depend upon the experimental resolution whether these peaks are separately observed or not. The clusters with valence electrons less than 3000 have

the largest l-value less than 20 and have only a limited amount of the degeneracy, and therefore clear differences in the number of degenerate states in the main- and sub-shells exist. Consequently, if two shells could be separated in experiments, the peaks (or minima) would be not equally spaced as a function of $N^{1/3}$. This finding strongly suggests that the equally spaced magic numbers observed by Lerme et al. are not due to the classical five-point star orbit.

5.3. Self-consistent jellium calculations

The properties of large alkali metal clusters can be described using the jellium model. The interacting valence electrons move in an external potential provided by a homogeneous positive background charge. At the cluster surface the background charge goes abruptly to zero. The jellium model has been mainly used for spherical clusters but also nonspherical small clusters have been studied[74]. The electronic many-body problem is usually solved using the Kohn-Sham method[75] with the local density approximation for the exchange and correlation energy[76]. The many-body problem then reduces to that of solving a single-electron Schrödinger equation

$$\left(-\frac{1}{2}\nabla^2 + V_{eff}(\mathbf{r})\right)\psi_i(\mathbf{r}) = \epsilon_i\psi_i(\mathbf{r}), \tag{38}$$

where the one-particle effective potential $V_{eff}(\mathbf{r})$ is the sum of the electrostatic potential ϕ and the local exchange-correlation potential μ_{xc}:

$$V_{eff}(\mathbf{r}) = -\phi(\mathbf{r}) + \mu_{xc}(n(\mathbf{r})), \tag{39}$$

where the electron density is

$$n(\mathbf{r}) = \sum_{i}^{N} |\psi_i(\mathbf{r})|^2. \tag{40}$$

The self-consistent equations are solved by a numerical iteration. The electronic shell structure can be seen in the density of states of the single-particle energies ϵ_i. The

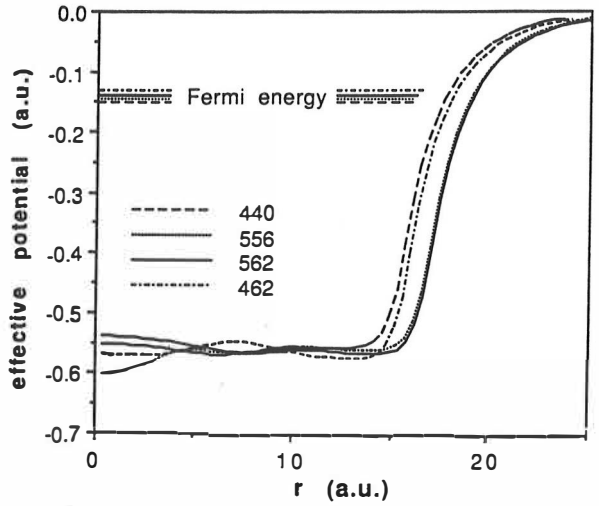

Fig. 26. The self-consistent effective potential of the jellium model for four different Al clusters.

self-consistent effective potential V_{eff} can be directly compared to the Woods-Saxon potential.

The electronic properties of Na clusters have been estimated[27] from the self-consistent jellium model. This model explained the experimentally observed supershell structure very well[27]. We have used the jellium model to study the shell structure in large Al clusters. The degeneracy with the ratio 2 : 5 was observed in the level structure of 440 and 462 electron Al clusters only in a limited low-energy part of the spectrum[77] and does not play any significant role in the shell structure. Related results have been provided recently by a jellium-model calculation for Al clusters[28], which produced a similar shell structure as for alkali-metal clusters and no signature of the classical star orbit was seen.

Figure 26 shows the effective potential for jellium clusters corresponding to the density of Al ($r_s = 2.07$). The softness of total self-consistent potential outside the cluster radius ($r > r_0$) is fairly insensitive to the potential inside. We can then conclude that the jellium-based models for Al clusters give potentials which are not soft enough for making the classical star orbit important. The exact shape of the potential is sensitive to the number of electrons in the cluster. This is due to the fact that only a small number of levels give dominant contributions to the density. However, the softness of the potential outside the surface is insensitive to the number

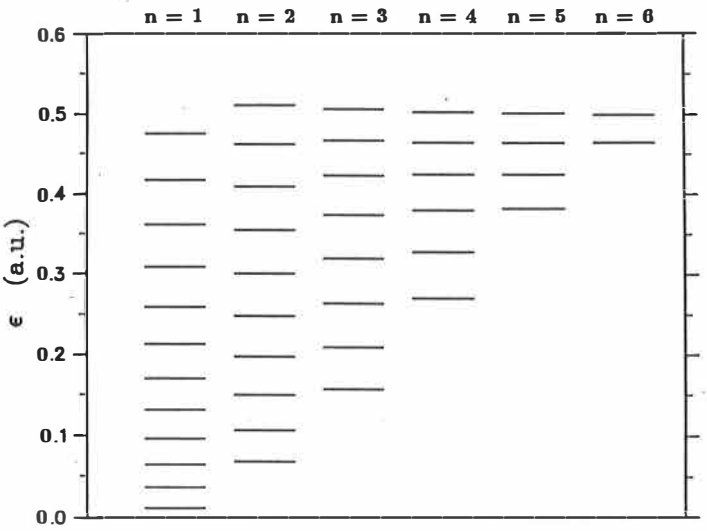

Fig. 27. The level spectrum of the mixed AlNa cluster.

of electrons. The same is true for the self-consistent electron density in the surface region, but the Friedel oscillations inside the cluster depend sensitively on exact number of electrons in the cluster. Outside the jellium surface (r_0) the effective potential corresponds to the Woods-Saxon potential with a softness parameter $\alpha =$ 0.6. On the other hand, inside the jellium radius the potential is clearly harder, corresponding to the Woods-Saxon potential with a large α-value.

The potential of a planar surface for high-density metals (small r_s) is harder than the potential for the low density metals (large r_s)[78]. However, in spherical clusters this is compensated with the smaller radius of the high-density metal clusters. The net effect is that the potential effectively becomes slightly softer for high-density metals (like Al) than for low-density metals (like Na). The shell structure changes in favour of the five-point star orbit by adding a low density Na ($r_s = 3.93$) positive background layer on the spherical high density Al ($r_s = 2.07$) cluster. The effective potential outside the jellium edge is then clearly softer than that of Al clusters. The Fermi energy which for Al clusters of the same size is at about –0.14 a.u., is for AlNa –0.11 a.u.. The electronic level energies for AlNa (450 electrons) are shown in Figure 27. The levels of $n = 1$ and 3 are degenerate with the ratio 2 : 5 at the Fermi level. Since the degeneracy of the levels of $n = 1$ and 2 with the ratio 1 : 3 is not completely broken at the Fermi level, the shell structure

is not entirely governed by the classical five-point star orbit, but it may be possible to extract the influence of the five-point star orbit.

6. Solids composed of metal clusters

6.1. Bandstructure calculation for cluster materials

Atomic clusters can serve as a source of new materials with uncommon properties[32]. The crystalline structure could be assembled from the magic metal clusters[33]. The electronic, optical, magnetic and structural properties of clusters are size specific. The possibility that materials with desired properties can be made by changing the size and composition of cluster aggregates is limitless. However, it is difficult to produce large quantities of clusters of specific size, and the clusters can interact with each other and coalesce to form larger clusters thus destroying the original properties. Khanna and Jena[33] have shown that it is possible to select clusters in such a way that the cluster-cluster interaction can be very weak. They suggested $Al_{12}Si$ as a candidate of clusters which would be used in assembling new materials where the clusters retain their identity. It has a compact icosahedral geometry and a closed electronic shell due to its 40 valence electrons. In the case of monovalent metals, the 8 atomic alkali clusters have a high symmetry, whereas in the case of 20 atom cluster the situation is still unclear[79,80].

The key requirement for the possibility of weakly bonded cluster material is the existence of narrow energy bands. We assume that the simple metal clusters with a closed electronic shell are nearly spherical and can be adequately described with the spherical jellium model. The self-consistent potential is then nearly constant inside the cluster and be reasonably approximated with a square well

$$V(r) = -V_0\theta(R - r), \tag{41}$$

where $V_0 = -\Phi - \epsilon_F$, Φ being the work function of the metal, ϵ_F the Fermi energy and R is the cluster radius, $R = r_s N^{1/3}$.

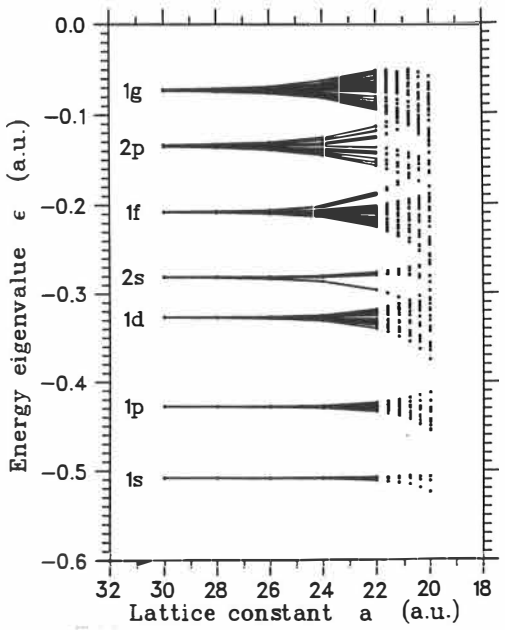

Fig. 28. Energy eigenvalues of $Al_{12}Si$ cluster material as a function of the lattice constant. The different energy bands are denoted by the single electron states in a single potential well. The Fermi energy is between $2p$ and $1g$ bands.

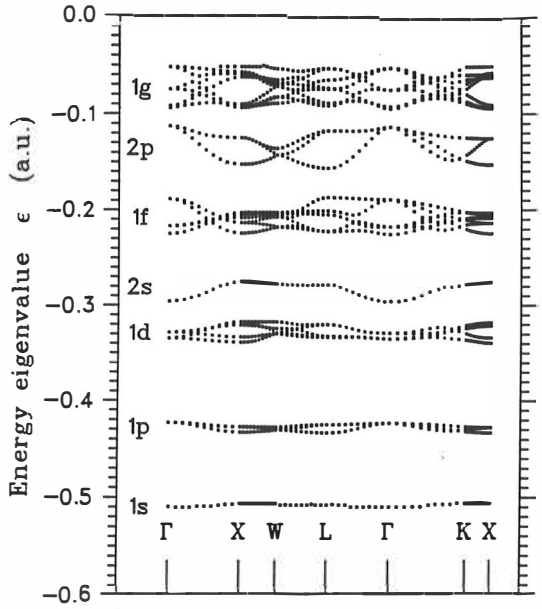

Fig. 29. Energy bands for fcc $Al_{12}Si$. The lattice constant is 22 a.u.

The cluster assembled material is approximated by making a lattice of the potentials of the individual clusters. Since the van der Waals bonded materials have

a tendency to form closed packed structures we consider only the fcc lattice. The electronic band structure is solved using a plane wave basis. Due to the simplicity of the potential a good accuracy has been obtained with about 2000 plane waves.

Figure 28 shows the development of the energy bands from the discrete cluster energy levels when the lattice constant becomes smaller. The figure is obtained by computing the energy eigenvalues for five high symmetry points (Γ, X, W,L and K) in the Brillouin zone. The Fermi energy lies in the gap between the $2p$ and $1g$ states. These bands start to overlap when the lattice constant is about 21.2 a.u.. The distance between the neighbouring potential wells is at that point about 1.0 a.u.. At so close distance the Al-Al distance between the neighbouring clusters would be smaller than the Al-Al distance within an $Al_{12}Si$ cluster. This means that if an fcc crystal is formed from $Al_{12}Si$ clusters it will be insulating. It is expected that the intercluster Al-Al distance in a weakly bonded cluster material is clearly larger than the intracluster Al-Al bond.

Figure 29 shows the band structure for $Al_{12}Si$ crystal with the lattice constant of 22 a.u.. The figure confirms that the band minima and maxima are obtained at the high symmetry points of the Brillouin zone. At the Fermi level the smallest gap is at the Γ-point, but the smallest gap can be also at other symmetry points or there can be an indirect gap as between $1d$ and $2s$ shells. The effective mass of electrons m^* is

$$m^* = \frac{\hbar^2}{\frac{\partial^2 \epsilon}{\partial k^2}}, \tag{42}$$

where ϵ is the energy and k the wave vector. Numerically this is obtained from the difference of energy ($\Delta\epsilon$) and distance (Δk) of two successive calculated points around the Γ-point in Fig. 29. The effective masses of electrons at the bottom of the 'conduction band' ($1g$) are 0.42 and 0.26 and those of the holes of 'valence band' ($2p$) are 0.47 and 0.20. These values, as also the energy gap, correspond well to those of the common semiconductors.

6.2. Discussion on cluster materials

The overall bandstructure is insensitive to the details of the potential parameters. The results for Na_{20} and Na_8 cluster materials are qualitatively similar to those obtained for the model potential mimicing $Al_{12}Si$[81]. The use of the self-consistent effective potentials of the jellium model could slightly change the size of the band gap but it would not change the qualitative features obtained with the model potentials. The band structure calculations show that if an fcc crystal can be formed from nearly spherical metallic clusters it will have a band gap at the Fermi level. This gives a possibility of van der Waals bonded materials. The total energy of such a material would probably be larger than that of a homogeneous bulk metal or alloy. Khanna and Jena[33] have shown that two Mg_4 clusters form a weakly bound cluster molecule where the individual four atomic clusters are only slightly disturbed from their isolated structures. Saito and Ohnishi[82] have used the jellium model to study the interaction of two 19 atom sodium clusters. They also found a cluster molecule but due to the open electron shell the two clusters were strongly bound together at a relatively short distance.

The jellium model could be used to study the physisorption between two Na_{20} clusters. Pachero and Ekardt[83] have studied the van der Waals interaction between small sodium clusters in the jellium model. The asymptotic formula for the attractive potential would give an estimate of the possible binding energy between the clusters. Since sodium clusters are known to be fairly soft and the atoms are mobile already well below the melting temperature[80,84], it is then likely that the clusters would melt together in trying to assemble the cluster material.

A better candidate for a cluster assembled material would be $Al_{12}Si$ where the electronic magic number is accompanied with a compact highly symmetric icosahedral geometry. Unfortunately, the jellium model is not suitable in calculating the interaction between Al clusters, because the negative surface energy in the jellium model would always favour a cluster material as compared to a homogeneous jellium. It should be stressed that the repulsive interaction coming from the closed electron shells are needed for making the physisorbed state possible between two

$Al_{12}Si$ icosahedra. Without the electronic shell effects two icosahedra brought close to each other would immediately melt together forming one larger cluster[85]. The latest calculations seem to show that it is not possible to maintain the $Al_{12}Si$ clusters in a solid but the clusters will coalesce to a bulk Al metal with substitutional Si impurities[86].

7. Summary

The Hückel model for a cubic lattice was shown to be the same as the discretized free-electron model in the cubic mesh. It can be used to study the shell structure corresponding the free-electron model at low energies. Using this method it was shown that for a cube, octahedron, cubo-octahedron and Wulff polyhedron the shell structure is different from that of a sphere already when the number of electrons is less than about 100.

A tight binding model with s- and p-electrons was used to study the effects of the surface roughness on the shell structure. It was found that fcc clusters have always so rough surface that at the Fermi level the shell structure is disturbed although just below the Fermi energy it is clearly seen. An ensemble of clusters at a finite temperature can have an average density of states which shows the shell structure although all of the individual clusters do not have the same shell structure. The level spacing distribution of clusters at a finite temperature was a Wigner distribution with the width slightly smaller than expected from the bulk density of states.

A potential well was used to study the shell structure in icosahedral clusters and in liquid clusters. The icosahedral clusters have the same shell structure as a sphere up to about 1000 electrons. It was shown that the surface fluctuations in liquid clusters do not destroy the main electronic shell structure. The relative effect of the surface fluctuations on the shell structure becomes smaller when the cluster size increases.

Shell structure in the Woods-Saxon potential changes continuously from the

hard-wall limit to the harmonic-oscillator limit when the softness of the potential is increased. Investigations with both the Woods-Saxon potential and the self-consistent jellium model gave negative results to the suggestion[5,29] of the dominant contribution of the classical five-point star orbit to the shell structure of the Al clusters. However, the shell structure changes in favour of the five-point star orbit by adding a Na layer on the spherical Al cluster.

Bandstructure calculations with model potentials indicated that if cluster assembled crystals could be formed from spherical metal clusters they are expected to be semiconductors.

References

[1] Bjørnholm S., Pedersen J., Nucl. Phys. News **1**, 18 (1991)

[2] Bergmann T., Martin T. P., Schaber H., Rev. Sci. Instrum. **60**, 347 (1989); **60**, 792 (1989)

[3] Martin T. P., Bergmann T., Göhlich H., Lange T., Chem. Phys. Lett. **172**, 209 (1990)

[4] Pedersen J., Bjørnholm S., Borggreen J., Hansen K., Martin T. P., Rasmussen H. D., Nature **353**, 733 (1991)

[5] Lerme J., Pellarin M., Vialle J. L., Baguenard B., Broyer M., Phys. Rev. Lett. **68**, 2818 (1992)

[6] Pellarin M., Lerme J., Baguenard B., Perez A., Broyer M., Vialle J. L., submitted

[7] Martin T. P., Näher U., Schaber H., Chem. Phys. Lett. **199**, 470 (1992)

[8] Martin T. P., Bergmann T., Göhlich H., Lange T., Chem. Phys. Lett., **176**, 343 (1991)

[9] Bjørnholm S., Borggreen J., Echt O., Hansen K., Pedersen J., Rasmussen H. D., Phys. Rev. Lett. **65**, 1627 (1990)

[10] Göhlich H., Lange T., Bergmann T., Martin T. P., Phys. Rev. Lett. **65**, 748 (1990)

[11] Bjørnholm S., Borggreen J., Echt O., Hansen K., Pedersen J., Rasmussen H. D., Z. Phys. D **19**, 47 (1991)

[12] Martin T. P., Näher U., Bergmann T., Göhlich H., Lange T., Chem. Phys. Lett. **183**, 119 (1991)

[13] Martins J., Buttet J., Surf. Sci. **106**, 261 (1981)

[14] Hintermann A., Manninen M., Phys. Rev. B **27**, 7262 (1983)

[15] de Heer W. A., Knight W. D., Chou M. Y., Cohen M. L., Solid State Physics **40**, 93 (1987)

[16] Bjørnholm S., Contemp. Phys. **31**, 309 (1990)

[17] Chou M. Y., Cleland A., Cohen M. L., Solid State Comm. **52**, 645 (1984)

[18] Manninen M., Solid State Commun. **59**, 281 (1986)

[19] Mayer M. G., Phys. Rev. **75**, 1969 (1949)

[20] Haxel O., Jensen J. H. D., Suess H. E., Phys. Rev. **75**, 1766 (1949)

[21] Knight W. D., Clemenger K., Heer W. A. de, Saunders W. A., Chou M. Y., Cohen M. L., Phys. Rev. Lett. **52**, 2141 (1984)

[22] Knight W. D., de Heer W. A., Clemenger K., Saunders W. A., Solid State Comm. **53**, 445 (1985)

[23] Katakuse I., Ichihara T., Fujita Y., Matsuo T., Sakurai T., Matsuda H., Int. J. Mass. Spectrom. Ion. Phys. **67**, 229 (1985)

[24] Balian R., Bloch C., Ann. Phys. **69**, 76 (1971)

[25] Nishioka H., Hansen K., Mottelson B. R., Phys. Rev. B **42**, 9377 (1990)

[26] Genzken O., Brack M., Phys. Rev. Lett. **67**, 3286 (1991)

[27] Brack M., Genzken O., Hansen K., Z. Phys. D **21**, 65 (1991)

[28] Genzken O., Brack M., Chabanat E., Meyer J., to be published

[29] Stampfli P., Bennemann K. H., Z. Phys. D **25**, 87 (1992)

[30] Ludvig W., Falter C., *Symmetries in Physics*, (Springer, Berlin) 1988

[31] Kubo R., Kawabata A., Kobayashi S., Ann. Rev. Mater. Sci. **14**, 49 (1984)

[32] Kroto H. W., Heath J. R., O'Brien S. C., Curl R. F., Smalley R. E., Nature **318**, 162 (1985)

[33] Khanna S. N., Jena P., Phys. Rev. Lett. **69**, 1664 (1992)

[34] Krätschmer W., Lamb L. D., Fostiporoulos K., Huffman D. R., Nature **347**, 354 (1990)

[35] Hebard A. F., in *Physics and Chemistry of Finite Systems: From Clusters to Crystals*, eds. Jena P., Khanna S. N., Rao B. K., (Kluwer, Dortrecht) 1992

[36] Hückel E., Z. Physik **70**, 204 (1931)

[37] Wang Y., George T. F., Lindsay D. M., J. Chem. Phys. **86**, 3493 (1987)

[38] Lindsay D. M., Wang Y., George T. F., J. Chem. Phys. **86**, 3500 (1987)

[39] Lindsay D. M., Chu L., Wang Y., George T. F., J. Chem. Phys. **87**, 1685 (1987)

[40] Lindsay D. M., Wang Y., George T. F., J. Cluster Sci. **1**, 107 (1990)

[41] Mansikka-aho J., Manninen M., Hammarén E., Z. Phys. D **21**, 271 (1991)

[42] Ashcroft N. W., Mermin N. D., *Solid State Physics*, (Holt, Reinhard and Winston, New York) 1976

[43] Manninen M., Mansikka-aho J., Hammarén E., Europhys. Lett. **15**, 423 (1991)

[44] Messmer R. P., *The Nature of the Surface Chemical Bond*, eds. Rhodin Th. N.,

Ertl G., (North-Holland, Amsterdam) 1980

[45] Pavloff N., Hansen M. S., Z. Phys. D **24**, 57 (1992)

[46] Manninen M., Jena P., Europhys. Lett. **14**, 643 (1991)

[47] Heine V., Solid State Phys. **35**, 1 (1980)

[48] Manninen M., Nieminen R., *Pintafysiikka*, (Gummerus, Jyväskylä) 1988

[49] Häkkinen H., Mansikka-aho J., Manninen M., J. Phys. Condens. Mater. **3**, 7757 (1991)

[50] North J. A., Xie J., Freeman D. L., Doll J. D., Z. Phys. D **12**, 69 (1989)

[51] Boyer L. L., Broughton J. Q., Phys. Rev. B **42**, 11461 (1990)

[52] Raoult B., Farges J., de Feraudy M. F., Torchet G., Z. Phys. D **12**, 85 (1989)

[53] Kimura K., Phase Transitions **24-26**, 493 (1990)

[54] Hag R. U., Pandey A., Bohigas O., Phys. Rev. Lett. **48**, 1086 (1982)

[55] Bohigas O., Ciannoni M. -J., *Mathematical and Computational Methods in Nuclear Physics*, eds. Dehesa J. J., Gomel J. M. G., Polls A., *Lecture Notes in Physics*, Vol. 209 (Springer, Berlin) 1984

[56] Mehta M. L., *Random Matrices and the Statistical Theory of Energy Levels*, (Academic Press, New York) 1990

[57] Binder K., *Monte Carlo Methods in Statistical Physics*, (Springer, Berlin) 1979

[58] Robertson I. J., Payne M. C., Heine V., Europhys. Lett. **15**, 301 (1991)

[59] Christensen O. B., Jacobsen K. W., Nørskov J. K., Manninen M., Phys. Rev. Lett. **66**, 2219 (1991)

[60] Heerman D. W., *Computer Simulation Methods in Theoretical Physics*, (Springer, Berlin) 1986

[61] Merikoski J., private communication

[62] Ebner C., Phys. Rev. A **23**, 1925 (1981)

[63] Tanaka S., Sugano S., Phys. Rev. **34**, 6880 (1986)

[64] Bucher J. P., Xia P., Bloomfield L. A., Phys. Rev. B **42**, 10858 (1990)

[65] Tanaka S., Sugano S., Phys. Rev. **34**, 740 (1986)

[66] Ratcliff K. F., *Multivariable Analysis V*, ed. Krishnaiah P. R., (North-Holland, Amsterdam) 1980

[67] Martins J. L., Z. Phys. D **12**, 347 (1989)

[68] Engel E., Perdew J. P., Phys. Rev. B **43**, 1331 (1991)

[69] Clemenger K., Phys. Rev. B **32**, 1359 (1985)

[70] Penzar Z., Ekardt W., Z. Phys. D **17**, 69 (1990)

[71] Hamamoto I., Mottelson B., Xie H., Zhang X. Z., Z. Phys. D **21**, 163 (1991)

[72] Mansikka-aho J., Hammarén E., Manninen M., Phys. Rev. B **46**, 12649 (1992)

[73] Bohr A., Mottelson B. R., *Nuclear Structure, Volume II*, (Benjamin, London) 1975

[74] Penzar Z., Ekardt W., Z. Phys. D **19**, 109 (1991)

[75] Kohn W., Sham L. J., Phys. Rev. **140**, A 1133 (1965)

[76] Jones R. O., Gunnarsson O., Rev. Mod. Phys. **61**, 689 (1989)

[77] Mansikka-aho J., Manninen M., Nishioka H., submitted in Phys. Rev. B

[78] Lang N. D., Kohn W., Phys. Rev. B **1**, 4555 (1970)

[79] Bonačič-Koutecký V., Fantucci P., Koutecký J., Chem. Rev. **91**, 91 (1991)

[80] Röthlisberger U., Andreoni W., J. Chem. Phys. **94**, 8129 (1991)

[81] Manninen M., Mansikka-aho J., Khanna S. N., Jena P., Solid State Comm. **85**, 11 (1993)

[82] Saito S., Ohnishi S., Phys. Rev. Lett. **59**, 190 (1987)

[83] Pachero J. M., Ekardt W., Phys. Rev. Lett. **68**, 3694 (1992)

[84] Ballone P., Andreoni W., Car R., Parrinello M., Europhys. Lett. **8**, 73 (1989)

[85] Valkealahti S., unpublished

[86] Seitsonen A. P., Puska M. J., Alatalo M., Nieminen R. M., Milman V., Payne M. C., submitted